Genetics and Molecular Mechanisms Underlying Congenital Mirror Movements

Meagan Collins

Integrated Program in Neuroscience (IPN)

Faculty of Medicine

McGill University, Montreal

A thesis submitted to McGill University in

partial fulfillment of the requirements of the degree of

Master of Science (MSc.)

August, 2020

Table of Contents

List of Figures

Acknowledgements

I am forever grateful to have been mentored and supported throughout my master's education by my two spectacular and accomplished co-supervisors. Dr. Myriam Srour, I truly appreciate your dedication to your patients, staff, and students, as well as your dedication to your mission of uncovering the genetic causes of neurodevelopmental disorders. You have inspired me not only to be a productive scientist but also a compassionate clinician hopefully in the future. Dr. Kibar, I sincerely appreciate your expertise and drive for understanding molecular and developmental neuroscience. You have provided the support for me to develop as a young scientist and as a science communicator by always providing me ample feedback for ways to strengthen my skills and understanding in these areas. Together, you both have portrayed the roles of "axonal guidance cues" for my life, aiding me while I navigate my path toward the completion of my degree and beyond.

Additionally, I am grateful to the Italian patient family for their participation in this study, as well as our collaborator, Dr. Alfonso Fasano, for initiating the recruitment of this family and carrying out early clinical characterizations. I would like to thank Mingqin Wang and Marie-Claude Guyot for their incredible dedication to this project, because without them, this work would not be possible. A special thanks to Judith St-Onge, Dr. Nassima Boudrahem-Addour, and the Bioinformatics team at the RI-MUHC for their support and immense dedication to this work. I would also like to thank Dr. Eric Samarut and Dr. Uday Kundap for their assistance with the behavioral assays for this project in the laboratory of Dr. Pierre Drapeau. I would also like to thank my advisory committee members Dr. Loydie Jerome-Majewska and Dr. Jean-Baptiste Rivière, as well as my IPN mentor Dr. Pierre Lachapelle for their guidance and support. Additionally, I would like to thank my friends and fellow lab mates at CHU-Sainte

Justine and the RI-MUHC for their support including: Claudie Comeau, Stephanie Vanier, Eric Krochmalnek, Dr. Sarah Alsubhi, Clara Lloyd, Anne Marie Fortuin, Sandrine St-Onge, Eve Racette, and Devanshi Shah.

I would also like to express my immense gratitude to the funding agencies that have supported my graduate education and this work including the Grand défi Pierre Lavoie Foundation, McGill University Faculty of Medicine, UQAM CERMO-FC, Montreal Children's Hospital Foundation, CIHR, Rare Disease Models and Mechanisms Network, and SickKids Foundation.

Abstract

Background: Congenital Mirror Movements (CMM) is a rare neurodevelopmental disorder, characterized by involuntary movements from one side of the body that mirror voluntary movements on opposite side. Some forms of CMM are inherited in an autosomal dominant fashion. Mutations in four genes have been associated with CMM cases: *DCC*, *RAD51*, *NTN1* and *DNAL4*. Together, these genes explain only approximately one third of cases, suggesting the possible existence of additional genes contributing to CMM. The purpose of this study is to validate the role of a new candidate gene *ARHGEF7* in the pathogenesis of CMM.

Methods: We have performed whole exome sequencing in a large autosomal dominant family with CMM and identified *ARHGEF7* (Gene ID: 8874) as a candidate gene. *ARHGEF7* encodes the Rho guanine nucleotide exchange factor 7, which plays a role in regulating cell polarity, adhesion and migration. We created a knock-out zebrafish mutant at the same site as in the human *ARHGEF7* variant identified in our CMM family. Using CRISPR-Cas9 technology, we have created a CRISPR-induced knockout mutant of both zebrafish orthologues of *ARHGEF7* (*arhgef7a* (Gene ID: 553493) and *arhgef7b* (Gene ID: 494081)). Behavioral analyses of both wild-type and mutant larvae were performed, particularly looking for evidence of involuntary turns on the inappropriate body side in response to startle, a mirror movement-like defect**.** Immunostaining with the anti-neurofilament M antibody αRMO44 was performed on wild-type zebrafish embryos to assess axonal migration.

Results: Mutant *arhgef7a* and *arhgef7b* zebrafish exhibited some mirror movement-like patterns in response to startle.

Conclusion: Our results suggest that the variant in *ARHGEF7* may contribute to the pathogenesis of CMM in this family.

Résumé

Contexte: Les mouvements miroirs congénitaux (MMC) sont un désordre neurodéveloppemental rare, caractérisé par des mouvements involontaires d'un côté du corps qui reflètent les mouvements volontaires du côté opposé. Certaines formes de MMC sont héritées d'une manière autosomique dominante. Des mutations dans quatre gènes ont été associées à des cas de MMC: *DCC*, *RAD51*, *NTN1* et *DNAL4*. Toutefois, l'ensemble de ces gènes n'explique qu'environ un tiers des cas, indiquant l'existence potentielle d'autres gènes contribuant aux MMC. Le but de cette étude est de valider le rôle d'un nouveau gène *ARHGEF7* dans la pathogenèse des MMC.

Méthodes: Nous avons effectué le séquençage entier de l'exome dans une grande famille autosomique dominante avec MMC et identifié *ARHGEF7* (ID de gène: 8874) comme gène candidat. *ARHGEF7* code pour le facteur d'échange nucléotidique Rho guanine 7, ayant un rôle dans la régulation de la polarité, l'adhésion et la migration cellulaires Nous avons introduit la variante *ARHGEF7* identifiée dans notre famille MMC dans un modèle de poisson zèbre. En utilisant la technologie CRISPR-Cas9, nous avons créé un mutant *knockout* des deux orthologues de *ARHGEF7* (*arhgef7a* (ID de gène: 553493) et *arhgef7b* (ID de gène: 494081)) du poisson zèbre. Nous avons mené des analyses comportementales sur le type sauvage et mutant visant la recherche d'un défaut analogue à un mouvement miroir. Nous nous sommes particulièrement intéressés à la détection de retournements involontaires du coté inapproprié du corps suite à un effet sursaut. L'immunocoloration avec l'anticorps anti-neurofilament M αRMO44 a été réalisée sur des embryons de poisson zèbre de type sauvage pour évaluer la migration axonale.

Résultats: Le poisson zèbre mutant *arhgef7a* et *arhgef7b* présentait des motifs semblables à des mouvements de miroir en réponse à un effet sursaut**.**

Conclusion: Nos résultats suggèrent que la variante de *ARHGEF7* pourrait contribuer à la pathogenèse des MMC dans cette famille.

Contributions of Authors

Chapter I: Meagan Collins wrote the general introduction and created the figures and tables under the supervision of Dr. Myriam Srour and Dr. Zoha Kibar. The patient family was clinically characterized by Dr. Alfonso Fasano, who subsequently sent samples to Dr. Srour's laboratory for further analysis. Dr. Srour screened the samples for mutations in known MM genes before sending the samples for whole exome sequencing. Blood samples were then sent for whole exome sequencing, and the filtering of variants was performed at the RI-MUHC by Dr. Srour using Dr. Guy Rouleau's pipeline. Samples were prepared by Judith St-Onge for Sanger sequencing validation. Dr. Srour and Judith St-Onge screened the patients in our CMM cohort for variants in the known CMM genes. Judith St-Onge screened additional patients with unexplained CMM for variants in *ARHGEF7*. Dr. Myriam Srour examined and collected clinical information for the patients in the CMM cohort. Judith St-Onge and Dr. Nassima Boudrahem-Addour assisted with collecting and organizing the general clinical information for the patients in the CMM cohort.

Chapter II: Meagan Collins wrote the methodology section, created the figures, performed the cloning and mutagenesis experiments, conducted the behavioral experiments, performed the immunohistochemical assays, and conducted the statistical analyses. Mingqin Wang designed and microinjected the CRIPR-Cas9 gRNA for the *arhgef7a* and *arhgef7b* zebrafish lines and maintained and genotyped the F0 generations of both lines. Judith St-Onge assisted with the preparation of cDNA for the cloning experiment. Mingqin Wang designed and assisted with the troubleshooting strategy for the *ARHGEF7* cloning experiment. Marie-Claude Guyot assisted the cloning experiment, general laboratory procedures, and with the immunohistochemical analyses. Dr. Eric Samrut and Dr. Uday Kundap assisted with the set-up of the behavioral assays. Dr.

Myriam Srour and Dr. Zoha Kibar designed the study, supervised the project, and provided essential feedback.

Chapter III: Meagan Collins wrote the results section, created the figures, genotyped the zebrafish from the F1 and F2 generations of both lines, performed all behavioral and immunohistochemical assays, and conducted the statistical analyses. Mingqin Wang assisted with the genotyping analysis and screening of the F1 and F2 generations of both lines. Marie-Claude Guyot assisted with general laboratory procedures and with the immunohistochemical analyses and imaging of the zebrafish. Dr. Eric Samrut and Dr. Uday Kundap assisted with the behavioral assays. Dr. Myriam Srour and Dr. Zoha Kibar supervised the project and provided important feedback.

Chapter IV: Meagan Collins wrote the general discussion under the supervision of Dr. Myriam Srour and Dr. Zoha Kibar.

Note Regarding the Impact of COVID-19

Due to the challenges regarding the COVID-19 pandemic, laboratories at the RI-MUHC, CHU-Sainte Justine, and the CR-CHUM were closed, and experiments were halted by mid-March 2020. This resulted in the incompletion of some planned experiments, including *in situ* hybridization assays, overexpression assays, RT-qPCR analysis, and additional behavioral experiments, that were to be included in this manuscript. Dr. Myriam Srour and Dr. Zoha Kibar acknowledge and approve of the processing of this thesis, considering the aforementioned situation. The Integrated Program in Neuroscience (IPN) at McGill University is also aware of the circumstances and have agreed to allow the evaluation of this thesis.

Chapter I: General Introduction

1.1 Overview

In 2007, a large Quebec family consisting of four generations was identified with numerous family members displaying a neurological phenomenon known as congenital mirror movements (CMM), whereby voluntary movements on one side of the body were accompanied by concurrent involuntary movements on the opposite side (Srour et al., 2009). A mono-allelic pathogenic variant in the *Deleted in Colorectal Carcinoma* (*DCC*) gene was later identified in all of the affected and some of the non-affected individuals from this family, indicating segregation of the mirror movement (MM) phenotype (Srour et al., 2010). This variant is suggestive of autosomal dominant inheritance with incomplete penetrance. Since 2010, pathogenic variants in three other genes (*RAD51*, *DNAL4*, *NTN1*) have been identified and linked to CMM (Depienne et al., 2012; Ahmed et al., 2014; Méneret et al., 2017).

Beginning in 2010 and continuing to 2014, a large Italian family was assessed for CMM (Fasano et al., 2014). DNA samples were collected from all available individuals and all individuals were screened for mutations in the four genes causing CMM: *DCC*, *RAD51*, *NTN1*, and *DNAL4*. No pathogenic variants segregating with MM were found in these genes. This led Dr. Myriam Srour and her colleagues to conduct whole exome sequencing. As a result, a rare heterozygous frameshift variant (NM_001113511.1:c.1751_1752delAC, p.Asn584Thrfs*90), was found in *ARHGEF7* in affected family members. *ARHGEF7* encodes the Rho guanine nucleotide exchange factor 7, which plays a role in regulating cell polarity, adhesion, and migration (Zhou et al., 2016). We screened our cohort of 35 individuals with unexplained CMM, but we did not identify any additional individuals carrying rare potentially pathogenic variants in *ARHGEF7*. Therefore, functional testing is required to validate the role of the identified variant in *ARHGEF7*

in the pathogenesis of CMM. The purpose of the present study was to validate the role of *ARHGEF7* in the pathogenesis of CMM using a knock-out zebrafish model.

1.2 Mirror Movements

Mirror Movements (MM) appear when voluntary movements from one side of the body are mirrored by involuntary movements on the opposite side of the body. For example, if a patient taps the fingers of their left hand together, their right hand will perform the same movement involuntarily. In addition, patients have difficulty performing unimanual tasks (Galléa et al., 2011). Some relevant examples of these problematic daily unimanual tasks include opening jars, typing, writing, and driving while shifting gears with the opposite hand (Galléa et al., 2011). MM have been mainly described for the upper limbs, especially for finger and hand movements, but they can also be observed in the lower limbs (Galléa et al., 2011). The severity of MM is clinically assessed according to the Woods and Teuber rating scale, an observation-based scale from zero ("No MM") to four ("MM equal to that observed in the intended hand") (Woods & Teuber, 1978). The severity of MM does not improve with age and is thus conserved across the lifespan (Galléa et al., 2011).

Physiological MM are mild MM which can be present during the early stages of development (Cox et al., 2012; Méneret et al., 2015). However, unlike pathogenic CMM, physiological MM normally resolve during childhood, usually by age seven, after the completion of the myelination of corpus callosum (inhibitory callosal connection) and the regression of the ipsilateral corticospinal tract (Bonnet et al., 2010; Demirayak et al., 2018). Moreover, these physiological MM are not usually simultaneous and are likely due to abnormal transcallosal inhibition, or the suppression of a hemisphere by the opposite hemisphere of the brain (Li et al., 2013).

Additionally, MM can be associated with syndromes characterized by additional neurologic and structural abnormalities, with prominent abnormalities of midline of the nervous system. Some of these complex disorders include the X-linked Kallmann syndrome (Krams et al., 1997; Mayston et al., 1997; Krams et al., 1999), the autosomal recessive Joubert syndrome (Ferland et al., 2004), and a musculoskeletal condition known as Klippel-Feil syndrome (Gunderson and Solitare, 1968; Farmer et al., 1990; Galléa et al., 2011). X-Linked Kallmann syndrome is caused by variants in *KAL1* gene, also known as the *ANOS1* gene (Galléa et al., 2011; Hardelin & Young, 2013). Joubert syndrome has been linked to pathogenic variants in numerous genes including *C5ORF42* and *TMEM231* (Brancati, Dallapiccola, & Valente, 2010; Srour et al., 2012; Srour et al., 2012). Klippel-Feil syndrome has been linked to variants in the genes *GDF6*, *GDF3*, and *MEOX1* (Karaca et al., 2015). Pathogenic early-onset MM which persist into adulthood, with no additional neurologic abnormalities present, are classified as isolated CMM, as described in the family of the present study (Demirayak et al., 2018).

1.3 Neurophysiology of Mirror Movements

The underlying neurophysiology of the corticospinal tract contributes to our understanding of Mirror Movements.

1.3.1 Corticospinal Tract

Fine motor movements that are voluntary, predominantly of the distal extremity muscles, are coordinated by the corticospinal tract. Approximately 40% of the axons which comprise the corticospinal tract project from the motor cortex, by the internal capsule and cerebral peduncle, to the medullary pyramids (Kandel et al., 2012). The axons then proceed to cross the midline at the pyramidal decussation and stop at the motor neurons of the ventral horn of the spinal cord (Kandel et al., 2012) (Figure 1). The majority of the axons of the corticospinal neurons (87%) in primates

decussate at the medullary pyramids (Rosenzweig et al., 2009). Those axons which do not decussate at the medullary pyramids cross at the spinal cord, whereas a few axons will remain ipsilateral (Rosenzweig et al., 2009). In rats, approximately 96-98% of the axons of the corticospinal neurons project to the contralateral side of the spinal cord (Rouiller et al., 1991).

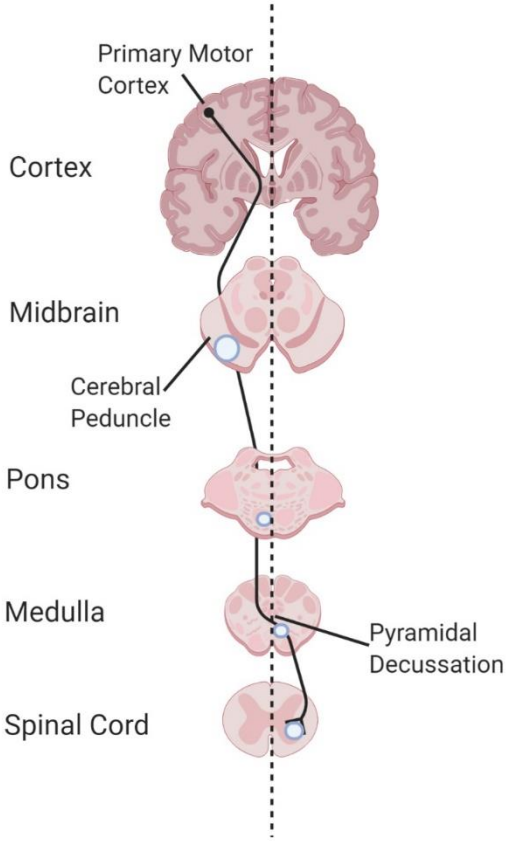

Figure 1. Schematic of Normal Human Corticospinal Tract. Diagram depicting the trajectory of the descending corticospinal tract from the motor cortex to the spinal cord and pyramidal decussation at the medullary pyramids at the medulla-spinal cord junction. Adapted from Kandel et al. (2000). Created with BioRender.com.

1.3.2 Movement Coordination

Neuroimaging studies in humans have shown that unilateral movements of the hands are mainly correlated with higher levels of activation in the contralateral hemisphere, including the areas of the primary motor cortex, premotor cortex, supplementary motor area, and basal ganglia (Shibasaki et al., 1993). However, the cerebellum is largely activated in the ipsilateral hemisphere (Turner et al., 1998). Control of unilateral movements is regulated in part by the corpus callosum through inhibitory interhemispheric pathways (Beaulé et al., 2012). Patients with isolated CMM are unable to perform solely unilateral movements. However, most patients without a corpus callosum do not have mirror movements. Therefore, the corpus callosum is not the only area which regulates unimanual control.

Transcranial Magnetic Stimulation (TMS) studies, which involve stimulating the primary motor cortex, are a useful tool for assessment of corticospinal excitability and interhemispheric inhibition. These studies are usually accompanied by electromyographic (EMG) recordings of the hand muscles. When TMS studies are performed on a healthy individual, TMS would be applied to one hemisphere's primary motor cortex and the primary motor cortex of the contralateral hemisphere is stimulated. The stimulation results in excitation of the corticospinal tract, and therefore a motor response in the contralateral side (Ferbert et al., 1992). However, TMS studies performed on CMM patients have revealed bilateral motor responses in the limbs to unilateral stimulation of the primary motor cortex with reduced interhemispheric inhibition, suggesting the presence of ipsilateral corticospinal tracts in individuals with CMM (Konagaya et al., 1990; Cohen et al., 1991). Additionally, TMS studies on CMM patients have shown that there are rapid motor evoked potentials (MEPs) in both the contralateral and the ipsilateral muscles of the limbs (Maegaki et al., 2007; Srour et al., 2010) (Figure 2). These findings have also been confirmed with

functional magnetic resonance imaging (fMRI) data, which have demonstrated that there is abnormal signaling across the corpus callosum, causing a reduction in interhemispheric inhibition (Leinsinger et al., 1997). In summary, these studies suggest that there is an abnormal ipsilateral connection (given bilateral simultaneous motor responses), and that there are also abnormalities in the callosal interhemispheric pathways in CMM.

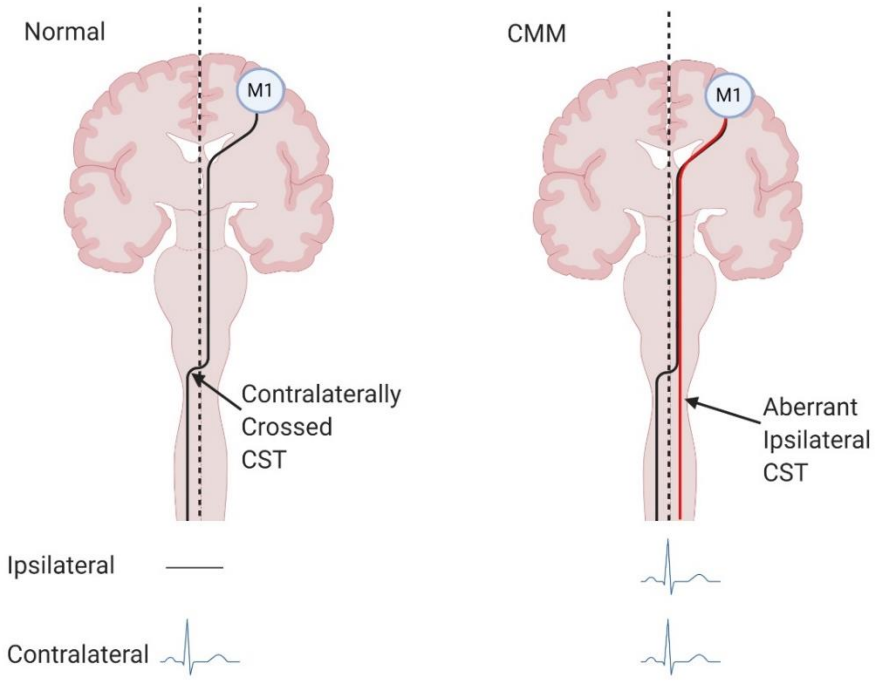

Figure 2. Schematic of Normal and CMM Corticospinal Tracts (CST) Decussation. Left: Normal CST tract. Right: CMM CST tract. M1 designates primary motor cortex. Black line indicates tracts facilitating voluntary movement, and red line shows MM tract. In CMM, there is the presence of the normal crossed tracks, but also abnormal ipsilateral tracts. Therefore, activation of the motor cortex results in normal movement of the contralateral limb through the normal crossed track, but also the ipsilateral limb, through the abnormal uncrossed tract. Adapted from Welniarz et al. (2015). Created with BioRender.com.

1.4 Axonal Guidance

Throughout neurodevelopment, axons navigate toward their respective targets. This process is executed by extracellular axon guidance cues. These cues include soluble, membrane-bound, and extracellular matrix molecules that are attractive or repellent for developing axons (Kandel et al., 2000). Moreover, axonal guidance cues work by inducing molecular changes in the growth cones, or growing ends, of developing axons (Dickson, 2002). Growth cones are considered as both sensory and motor structures, and they are comprised of a central core made of microtubules, finger-like extensions made of actin (filopodia), and jutting, ruffled sheets (lamellipodia) (Kandel et al., 2000). Growth cones extend, pull back, or change their direction during pathfinding by using the dynamics of their cytoskeletal proteins. Guidance cues work to alter the organization of the cytoskeleton (Kandel et al., 2000; Kalil and Dent, 2005; Dent et al., 2011). The process of axonal guidance plays an extremely important role in wiring and coordinating the connections of the brain (Kandel et al., 2000, Drachman, 2005). This complex process is completed with relatively few guidance cue families, some of which include netrins, slits, semaphorins, and ephrins (Kandel et al., 2000, Dickson, 2002).

CMM is considered a “disorder of axonal guidance”, due to the abnormal decussation of the motor corticospinal tract. Diffusion Tensor Imaging (DTI), an MRI technique allowing for the measurement of the diffusion of water in tissues, has revealed this abnormal decussation of the motor corticospinal tracts in individuals with CMM (Brandao et al., 2014).

1.5 Genetic Etiology of Mirror Movements

CMM can be familial or sporadic (Méneret et al., 2014). Pathogenic variants have been found in four known genes *DCC* (deleted in colorectal carcinoma; MIM*120470), *RAD51* (RAD51 recombinase; MIM*179617), *DNAL4* (dynein axonemal light chain 4; MIM* 610565), and *NTN1* (Netrin-1; MIM*601614) (Table 1).

Table 1: Description of Known CMM Genes

Gene Name	OMIM Number	Inheritance Pattern	Phenotype
DCC	MIM*120470	Autosomal Dominant	CMM
RAD51	MIM*179617	Autosomal Dominant	CMM
DNAL4	MIM* 610565	Autosomal Recessive	CMM
NTN1	MIM*601614	Autosomal Dominant	CMM

1.5.1 *DCC*

The first gene to be identified in the pathogenesis of CMM was the *Deleted in Colorectal Carcinoma* (*DCC*) gene (Srour et al., 2010). *DCC* was initially found to be deleted in colorectal cancers, as well as other somatic cancerous tumors. *DCC* is best known for its role in midline axonal guidance and the development of white matter projections throughout the central nervous system (Méneret et al., 2014). Mutations in *DCC* are also responsible for other more severe neurologic phenotypes in humans, such as agenesis of the corpus callosum, intellectual disability, and developmental split-brain syndrome (Marsh et al., 2017; Marsh et al., 2018; Jamuar et al., 2017).

DCC encodes the receptor to Netrin-1, a chemoattractant molecule that is expressed in the midline of the developing fetus (Kennedy et al., 1994). To date, all *DCC* variants reported in familial CMM have been loss of function mutations, leading to nonsense-mediated mRNA decay. A haploinsufficiency mechanism of action is suspected, whereby decreased amount of DCC levels are predicted to result in a decrease in ventral commissure of the spinal cord and corpus callosum (Srour et al., 2010).

DCC animal models have been used to assess the function of this gene contributing to the pathogenesis of CMM. For example, *Dcc* mice carrying a mutation deleting exon 29 are known as "kanga" mice because they show a hopping gait motion, analogous to the human MM seen in individuals with *DCC* mutations (Finger et al., 2002). Additionally, there are observed failures of midline crossing in the corticospinal tract for the homozygous *Dcc* "kanga" mice (Finger et al., 2002).

1.5.2 *RAD51*

The *RAD51* gene is involved in DNA repair and homologous recombination. Therefore, *RAD51* is essential for preserving genomic integrity (Depienne et al., 2012). *RAD51* has also been implicated in breast cancer. The RAD51 protein interacts with BRCA1 (*BRCA1* [MIM 113705]) and BRCA2 (*BRCA2* [MIM 600185]). Genomic instability and tumor development are thought to be a result from defective homologous recombination (Depienne et al., 2012).

In CMM patients, mutations in *RAD51* lead to atypical decussation of corticospinal tracts and bilateral activation in motor areas while unimanual actions are being performed (Depienne et al., 2012). In *Rad51* mice models, homozygous *Rad51* knockout zygotes had altered cell proliferation and irregular cell morphology (Depienne et al., 2012). These mice are also unable to undergo embryonic development after embryonic day 6 (Depienne et al., 2012). However,

heterozygous *Rad51* mice are viable, can reproduce, and have no visible defects, but the central nervous system (CNS) morphology and motor phenotype have not been investigated (Depienne et al., 2012). To date, there is no evidence suggesting that patients with CMM linked to variants in *RAD51* exhibit an increased risk for developing cancer.

1.5.3 *NTN1*

The *NTN1* gene encodes the ligand to *DCC*, and is involved midline crossing in the CNS, tumorigenesis, and inflammation. Netrin-1 belongs to a family of extracellular proteins which are important for the regulation of cellular migration (Kennedy et al., 1994). Netrin-1 protein is expressed at the midline of the central nervous system during development. Furthermore, it acts as an axonal guidance cue to attract or repulse various types of commissural axons (Méneret et al., 2017). Netrin-1 mainly functions locally by fostering growth cone adhesion. Patients with MM and mutations in *NTN1* have defects in corticospinal tract crossing (Méneret et al., 2017).

Hypomorphic *Ntn1*-mutant mice have reduced decussation of the CST, consistent with the uncrossed CST fibers observed in *NTN1* and *DCC*-CMM patients (Méneret et al., 2017). These mice mutants usually die soon after birth and show agenesis of the corpus callosum and defects in commissural axon projections (Méneret et al., 2017).

1.5.4 *DNAL4*

The *DNAL4* gene encodes an axonemal dynein light chain which is a part of the molecular motor complex and it provides the force to move cilia (Ahmed et al., 2014). Recessively inherited mutations in *DNAL4* in a single patient family with multiple consanguineous loops were implicated to play a role in the cytoplasmic dynein complex for Netrin-1-driven retrograde transport (Ahmed et al., 2014). However, functional studies have not been performed.

1.5.5 Human Mutations resulting in Mirror Movements

CMM mutations are usually inherited in an autosomal dominant fashion, yet some rare, autosomal recessive cases in only one family with multiple consanguineous loops have been reported with mutations in *DNAL4* (Ahmed et al., 2014). CMM can also occur sporadically, where a patient can present symptoms, with no previous family history of the disorder (Méneret et al., 2017). Most cases of CMM follow an autosomal dominant inheritance pattern, and incomplete penetrance, as well as, variable expressivity have been reported. Familial CMM mutations are usually incompletely penetrant, where some family members with the mutation have CMM and other family members with the same mutation are asymptomatic (Méneret et al., 2017). Furthermore, the severity of MM can be variable within a family (Galléa et al., 2011).

Variants in *DCC* are the most common. Variants in *RAD51* are the second most common, followed by a few previously reported variants in *NTN1* and *DNAL4* (Figure 3). Yet, previous studies have shown that approximately 35% of affected individuals have a pathogenic variant in either *DCC* or *RAD51* (Méneret et al., 2017). Mutation carriers of *RAD51* variants typically exhibit detailed mirror movements, such that their mirroring hand fully mirrors the voluntary hand, whereas those with *DCC* variants display "fractionated" mirror movements, where the mirroring movements are classified as more fragmented and saccadic (Franz et al., 2015). There have been three previously reported variants in *NTN1* change amino acids in the NTR (netrin) domain (Méneret et al., 2017). One homozygous splice site mutation has been previously reported in *DNAL4*, which results in the in-frame deletion of 28 conserved residues (Ahmed et al., 2014).

Dr. Srour's cohort consists of 119 individuals total, with 79 affected patients, representing the largest CMM cohort worldwide. There are 45 individuals from 17 families for which a molecular diagnosis has been identified. Variants in *DCC* were identified in 39 affected individuals

from 13 families (Fig. 1A). The most common variant in *DCC* was a frameshift variant (NM_005215.3: c.1140+1G>A, p.(Val329GlyfsTer15)), which was found in 14 affected individuals and 6 asymptomatic carriers (3 families) (Srour et al., 2009). In our cohort, two missense variants of unknown significance (VUS) were found in *RAD51*. One missense VUS (NM_001164270.1: c.551A>G, p.(Asp184Gly)) was found in one affected female (Fig. 1B). This variant is predicted as pathogenic by Mutation Taster and has not been reported in gnomAD. Another missense VUS (NM_001164270.1: c.401C>A, p.(Thr134Asn)) was identified in 3 affected individuals (Fig.1B). This variant is also predicted as pathogenic by Mutation Taster and has not been reported in gnomAD. A missense VUS in *NTN1* (NM_004822.2: c.1802G>C, p.(Cys601Ser)) was found for one affected male (Fig. 1C) and has been included in Méneret et al. (2017). This variant is predicted as pathogenic by Mutation Taster and has not been reported in gnomAD. A previously unreported variant of unknown significance has been found in *DNAL4* (NM_005740.2: c.104C>T, p.(Thr35Ile)) in one affected patient in our cohort. This variant is predicted as pathogenic by Mutation Taster and has not been reported in gnomAD. However, this variant does not explain CMM in this patient since MM due to *DNAL4* have a recessive mode of inheritance, and a second variant was not identified.

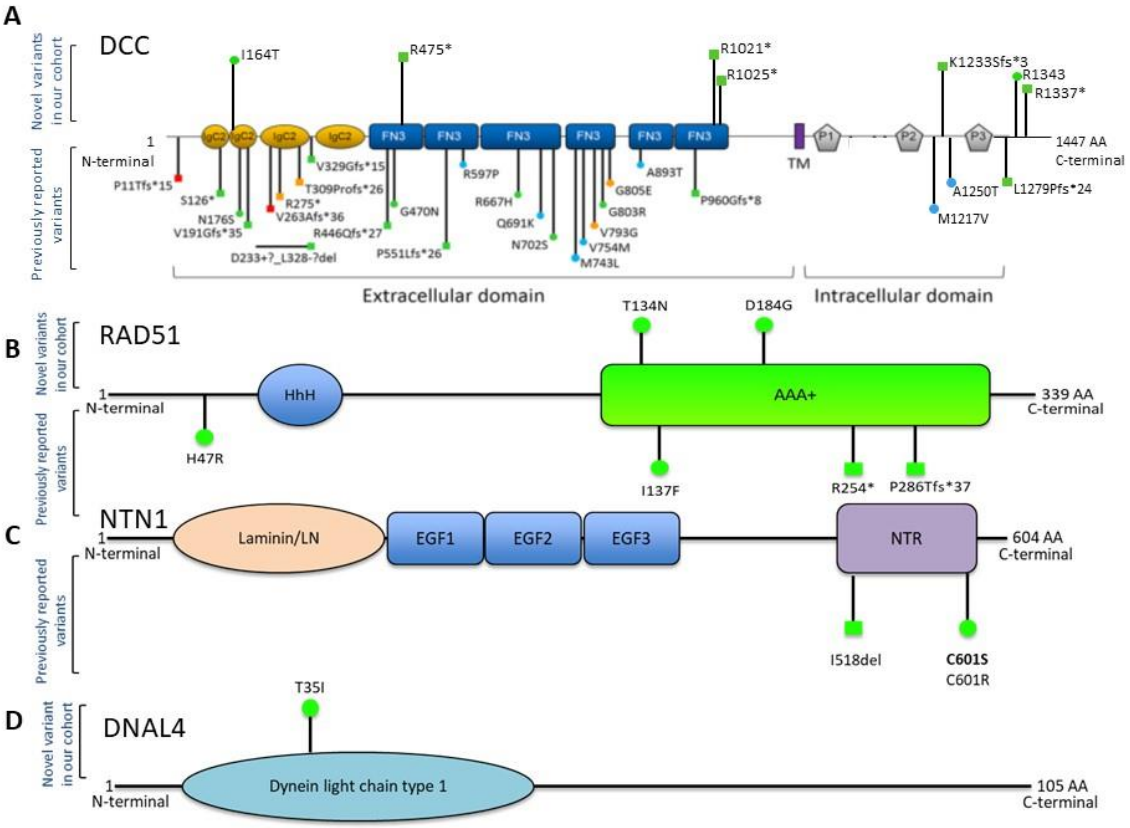

Figure 3. Distribution of CMM variants in DCC, RAD51, NTN1, and DNAL4 proteins.

(A) DCC. Square: predicted loss of function mutation; circle: missense mutation; green: mirror movement (MM); blue: agenesis of corpus callosum (ACC); orange: MM + ACC; red: developmental split-brain syndrome. Image modified from Marsh et al. (2017).

(B) RAD51. Helix-hairpin-helix domain (HhH) depicted in blue. ATPase domain (AAA+) shown in green. Square: predicted loss of function mutation; circle: missense mutation; green: mirror movement (MM).

(C) NTN1. Laminin N-terminal domain (domain VI) shown in coral, Laminin EGF domain (domain V) shown in blue, NTR domain (Netrin domain) shown in lavender. Square: predicted loss of function mutation; circle: missense mutation; green: mirror movement (MM). Bolded C601S variant is from our cohort and has been previously reported.

(D) DNAL4. Dynein light chain type 1 shown in turquoise. Square: predicted loss of function mutation; circle: missense mutation; green: mirror movement (MM).

1.6 Zebrafish as a Model Organism

Zebrafish (*Danio rerio*) are a valuable model organism for biological and biomedical research and the study of vertebrate gene function (Howe et al., 2013). The use of the zebrafish model has many benefits including that they are small and robust, they have the same major organs and tissues as humans, and the embryos of this species are virtually transparent. Additionally, zebrafish share approximately 70% of genes with humans (Howe et al., 2013). Furthermore, approximately 84% of human genes that are affiliated with human disease have a counterpart in zebrafish (Howe et al., 2013). This model also provides researchers the capacity to fast-track genetic studies by gene knockdown or overexpression.

1.6.1 Zebrafish Mauthner Hindbrain Neurons

Simpler vertebrates, such as zebrafish, have reticulospinal tract neurons which cross contralaterally and are analogous to the human corticospinal tract (Jain et al., 2014). This makes the zebrafish model a simplified system useful for analyzing descending motor control (Jain et al., 2014). In zebrafish, the Mauthner hindbrain array, which comprises M-cells and its homologs, the MiD2/MiD3 cells, is involved in the escape response (Colwill and Creton, 2012). Some of the ways to elicit startle responses are through tactile stimuli, acoustic stimuli, water flow changes, changes in light intensity, open areas, and moving objects (Colwill and Creton, 2012; Kalueff et al., 2013).

When using light stimuli, the startle response is typified by a short period of higher activity which is produced when light is suddenly turned off at 3 dpf (Easter and Nicola, 1996) or when light is suddenly turned on or off at 4 or 5 dpf (Emran et al., 2008).

1.6.2 Zebrafish *dcc* Mutants with Mirror Movement-like Defects

Zebrafish *spaced out* (*spo*) mutants carry *dcc* mutations, with a single amino acid substitution affecting the binding of Netrin. These *dcc* mutants (dcc^{ts239}, dcc^{tm272b}, and $dcc^{zm130198}$) have been shown to exhibit mirror movement-like defects (Jain et al., 2014). In this zebrafish model, *dcc*-mutant larvae exhibit involuntary turns on the wrong body side in response to unilateral tactile stimuli. It was shown that these mirror movement-like defects are linked to axonal guidance defects of commissural reticulospinal hindbrain neurons, where aberrant ipsilateral projections of MiD2/MiD3 reticulospinal hindbrain neurons activate the observed movements on the inappropriate body side (Figure 4) (Jain et al., 2014). Instead of crossing contralaterally, the axons of these reticulospinal neurons in *dcc* mutant zebrafish recurrently project ipsilaterally and do not cross the midline (Jain et al., 2014) (Figure 5).

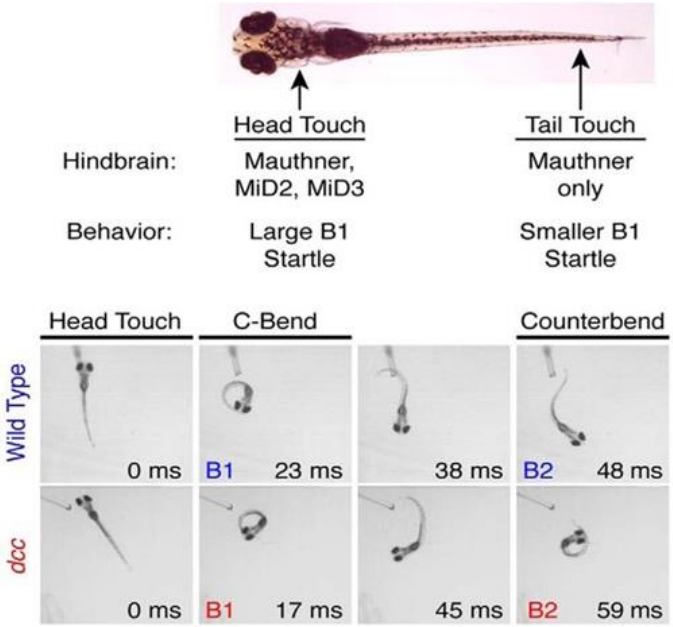

Figure 4. Touch-Evoked Startle Response Results. WT fish perform escape startle response C-bend and Counterbend. dcc mutants orient to the inappropriate body side. Adapted from Jain et al. (2014) (Permission for use granted by Journal of Neuroscience).

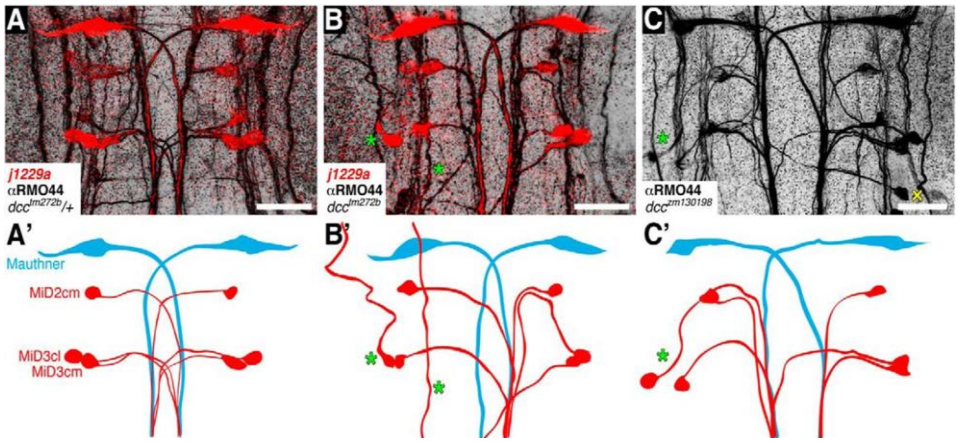

Figure 5. Confocal Axonal Projections of Hindbrain Interneurons. 60–70 hpf Zebrafish Embryos Immunostained with αRMO44 (Jain et al., 2014). A and A') *dcc* heterozygotes have normal neuronal projections. B and B') dcc^{tm272b} homozygous mutants have aberrant MiD2/MiD3 ipsilateral projections as indicated by green stars. C and C') $dcc^{zm130198}$ homozygous mutants have aberrant MiD2/MiD3 ipsilateral projections as indicated by green star. (Permission for use granted by *Journal of Neuroscience*).

1.7 Preliminary Data and Results

1.7.1 Italian Patient Family

A large multigenerational family with autosomal dominant CMM from Italy was phenotypically described by Dr. Alfonso Fasano et al (Fasano et al., 2014) (Figure 6). The affected family members have differing degrees of severity of the CMM phenotype, consistent with variable expressivity (Table 2).

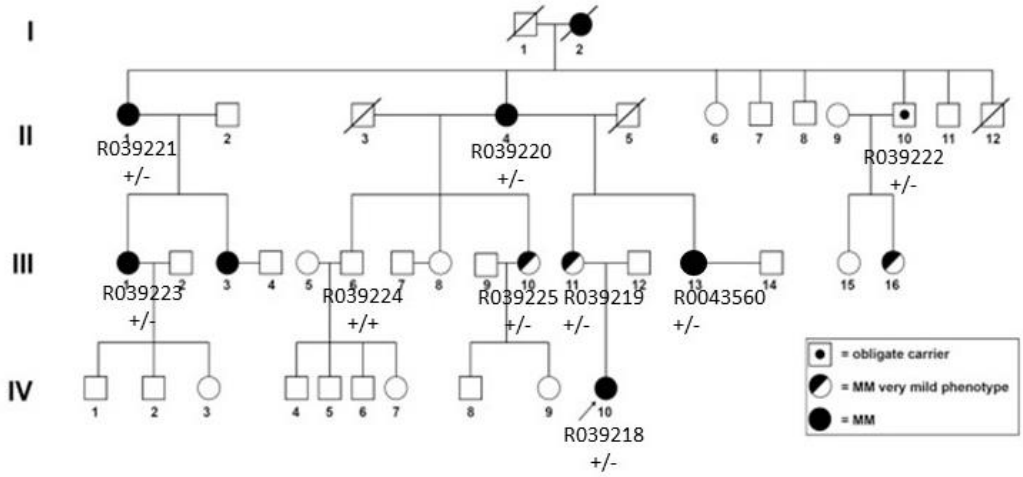

Figure 6. Pedigree of the CMM patient family depicting autosomal dominant inheritance with variable expressivity. Using whole exome sequencing, we found a rare heterozygous variant in *ARHGEF7* (Gene ID: 8874) that was shared by all affected family members (+/+=normal, +/-= heterozygous). R number corresponds to ID number listed in Table 1.

Table 2: Clinical Features of CMM Family

ID Number	Generation	Relationship	Clinical Status	Sex	DOB	Gene	Variant
R0039218	IV-10	Proband	Affected	F	2005/11/13	*ARHGEF7*	NM_001113511.1: c.1751_1752delAC, p.Asn584Thrfs*90
R0039219	III-11	Mother	Affected(mild)	F	1974/10/02	*ARHGEF7*	NM_001113511.1: c.1751_1752delAC, p.Asn584Thrfs*90
R0039220	II-4	Grandmother Mother of R39225+R39219	Affected	F	1950/01/06	*ARHGEF7*	NM_001113511.1: c.1751_1752delAC, p.Asn584Thrfs*90
R0039221	II-1	Grand Aunt	Affected	F	1939/03/05	*ARHGEF7*	NM_001113511.1: c.1751_1752delAC, p.Asn584Thrfs*90
R0039222	II-10	Grand Uncle	Affected (Obligate Carrier)	M	1955/02/06	*ARHGEF7*	NM_001113511.1: c.1751_1752delAC, p.Asn584Thrfs*90
R0039223	III-1	Aunt	Affected	F	1973/04/11	*ARHGEF7*	NM_001113511.1: c.1751_1752delAC, p.Asn584Thrfs*90
R0039224	III-6	Uncle	Normal	M	1970/02/05	Normal	Normal
R0039225	III-10	Half Aunt	Affected(mild)	F	1977/05/10	*ARHGEF7*	NM_001113511.1: c.1751_1752delAC, p.Asn584Thrfs*90
R0043557	-	Cousin	Normal	M	1993/09/22	*ARHGEF7*	NM_001113511.1: c.1751_1752delAC, p.Asn584Thrfs*90
R0043560	III-13	Aunt	Affected	F	1979/04/16	*ARHGEF7*	NM_001113511.1: c.1751_1752delAC, p.Asn584Thrfs*90

1.7.2 Genetic Screening

Three individuals (R0039221, R0039220, and R0039225) were initially screened for variants in *DCC* and *RAD51* (Fasano et al., 2014). These screenings did not identify any variants in *DCC* or *RAD51*. Additional screening of *DNAL4* and *NTN1* did not identify any rare variants.

Additional samples were obtained from the other available family members later (R0039218, R0039219, R0039222, R0039223, R0039224, R0043557, R0043560). Informed consent was obtained from all individuals. All procedures were approved by Research Ethics Committees of each respective institution.

DNA was isolated from whole blood samples obtained from the individuals using the Qiagen Puregene Blood Core C Kit (MD, USA). Primer pairs were designed with Primer 3 Plus for amplifying exonic regions and exon/intron boundaries. The 48 primer pairs were pooled in an 11 primer mix according to two characteristics: the distance between each pair should be more than 3 kb and the size of the amplicons should be different by 10% going from 300bp to 1.5 kb in a primer mix. Multiplex PCRs were performed in final volume of 25µL with 100ng DNA, 0.1 µM of each primer, 1x Platinum Multiplex PCR Master Mix (Life Technologies). Reactions were performed in C1000 Touch Thermal Cycler (Bio-Rad Laboratories). PCR products were visualized in 1% agarose gel. The 11 Multiplex PCRs from each patient were pooled together in a 50µL volume reaction. Subsequently, the PCRs were purified with Agencourt AMPure XP beads following the manufacturer protocols (Beckman Coulter, CA, USA).

Following the quantification of the pooled PCR reactions with Qubit 3.0 Fluorometer (Life Technologies), a dilution of 0.2 ng/µL was prepared. Library preparation with Illumina Nextera XT DNA Sample Preparation Kit (Illumina, Vancouver, Canada) was performed using

5µL, containing 1 ng of DNA. Libraries were then paired-end sequenced in reactions of 150-bp reads on the MiSeq using 300-cycle reagent kits (Illumina, Vancouver, Canada) and bioinformatic analyses were performed. This screening was negative for variants in all four known genes, suggesting that the CMM phenotype in this family was caused by a pathogenic variant in a novel CMM gene. Therefore, whole exome sequencing was performed to determine the cause of the CMM phenotype in this family.

1.7.3 Whole Exome Sequencing

Whole exome sequencing was performed on DNA extracted from blood from ten family members (7 affected (R0039221, R0039220, R0039225, R0039218, R0039219, R0039223, R0043560), 1 obligate carrier (R0039222), 2 unaffected (R0039224, R0043557)) (Figure 6, Table). After filtering for rare variants (MAF <1%) that were present in all affected family members and were absent in inhouse and external controls, variants were found in *KIF19* (NM_153209: c.G2567A), *OTOP3* (NM_178233: c.T1016C), and *ARHGEF7* (NM_001113511.1: c.1751_1752delAC) (Table 3).

Table 3: WES Variants

Gene Name	Exon	Variant	Position (Assembly GRCh37)	Zygosity	CADD Score	gnomAD allele frequency	SNP	In-silico Prediction Models (Polyphen, Mutation Taster, SIFT)	ACMG Classification
KIF19	Exon 18	NM_153209: c.2567G>A, p.Arg856Gln	chr17:72350559	Heterozygote	0.361707	1.5e-5	rs199686832	Benign	Likely Benign (BS1, BP4)
OTOP3	Exon 6	NM_178233: c.1016T>C, p.Phe339Ser	chr17:72942966	Heterozygote	3.204715	6.050e-5	rs150408824	Damaging	Likely Benign (BS1, BP4)
ARHGEF7	Exon 15	NM_001113511.1: c.1751_1752delAC, p.Asn584Thrfs*90	chr13:111932986	Heterozygote				Damaging	Likely Pathogenic (PVS1, PM2)

The variant found in *KIF19* (NM_153209: c.G2567A, p.R856Q) is predicted as benign/tolerated by Poly-phen-2 and Mutation Taster in silico prediction programs and has been reported in gnomAD with an allele frequency of 1.5e-5. The variant found in *OTOP3* (NM_178233: c.T1016C, p.F339S) is classified as a SNP variant (dbSNP (rs150408824)) and has been reported in gnomAD with an allele frequency of 6.050×10^{-5}. The heterozygous frameshift variant in *ARHGEF7* (NM_001113511.1: c.1751_1752delAC, p.Asn584Thrfs*90) replaces the last 219 amino acids with 90 abnormal amino acids (Gene ID: 8874) (Figure 7). This variant has not been previously reported, and it is predicted as damaging by Mutation Taster and is predicted to undergo nonsense-mediated decay by in silico prediction tools. This variant was the only rare, truncating variant found from the WES data that was absent in gnomAD. We screened our cohort of 35 individuals with unexplained CMM, but we did not identify any additional individuals carrying rare variants in *ARHGEF7*.

Figure 7. Depiction of protein domains for ARHGEF7. Mutation p.Asn584Thrfs*90 shown with arrow. Created with DOG 2.0 software (Ren et al., 2009).

1.7.4 Candidate Gene: *ARHGEF7*

The gene of interest in the present study, *ARHGEF7* (Gene ID: 8874), also known as *β-Pix* or *Cool1*, has been shown to be involved in cellular polarity, migration, and adhesion (Zhou et al., 2016). This gene is a member of the GIT-PIX complex, and it regulates the exchange of bound GDP for GTP. *ARHGEF7* has also been implicated in axon formation during cortical development (López Tobón et al., 2018).

Additionally, *ARHGEF7* has been linked to cancer through the regulation of motility of cancer cells by controlling the actin cytoskeleton and the promotion of metastasis of colorectal adenocarcinoma (Lei et al., 2018). Mutations in *ARHGEF7* have also been implicated in other cancers including breast cancer, gliomas, and primitive neuroectodermal tumour-medulloblastoma, as reported in COSMIC (Catalogue Of Somatic Mutations In Cancer) (Figure 8).

ARHGEF7 is widely expressed, with the highest expression levels present in the brain. *ARHGEF7* has four protein domains: the Calponin homology domain (CH), the SRC Homology 3 domain (SH3), the Dbl-homologous domain (DH), and the Pleckstrin Homology domain (PH) (Bustelo et al., 2007). The CH domain is about 100 amino acids long and it belongs to a family of actin binding domains located in both cytoskeletal and signal transduction proteins (Korenbaum & Rivero, 2002). The SH3 domain SRC Homology 3 Domain (or SH3 domain) is about 60 amino acids long and is a protein-protein interaction domain that is involved in the assembly of specific protein complexes (Kurochkina, & Guha, 2013). The DH domain is involved in Rho GTPase interaction and activation, and the PH domain is involved in intracellular targeting of the DH domain function (Zhu et al., 2001).

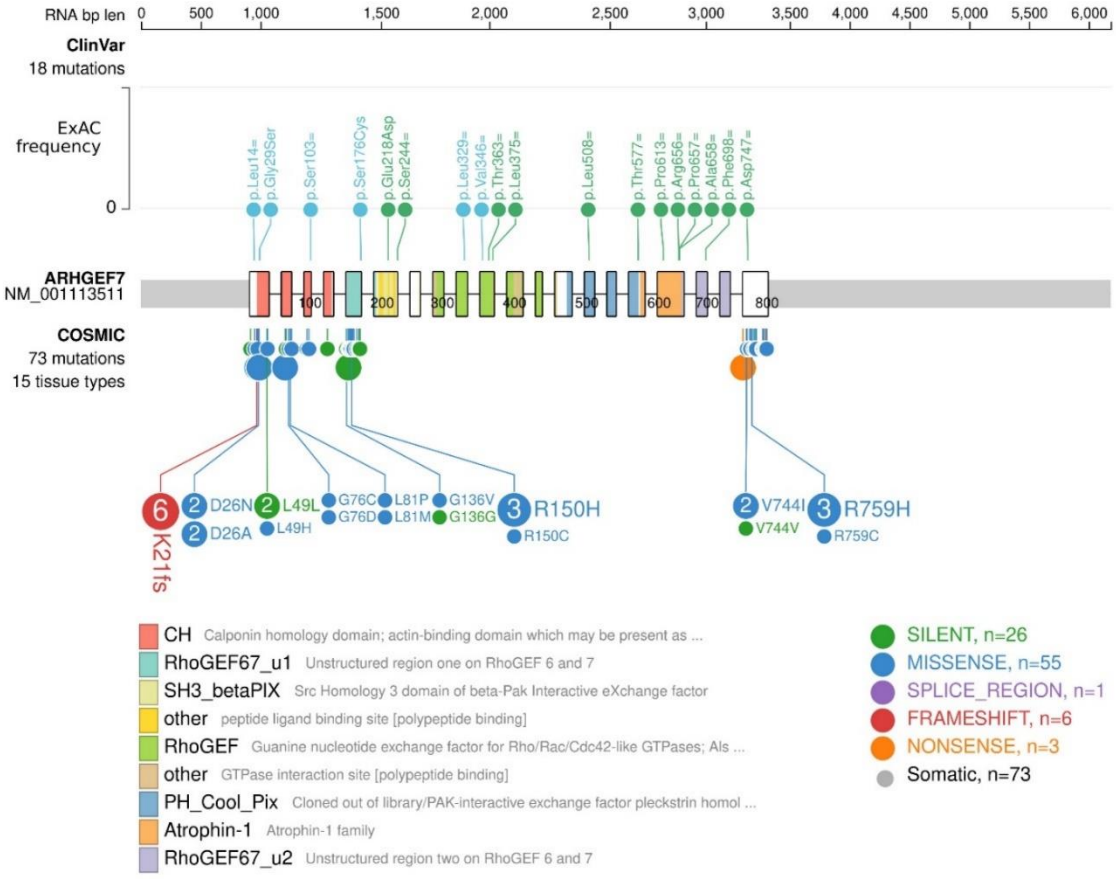

Figure 8. *ARHGEF7* previously reported variants in COSMIC and ClinVar. Most of the previously reported variants have been reported in COSMIC (Catalogue Of Somatic Mutations In Cancer). The most frequently reported type of mutations found in *ARHGEF7* are missense mutations (n=55), followed by silent mutations (n=26), frameshift mutations (n=6), nonsense mutations (n=3), and splice region mutations (n=1). Image was generated using ProteinPaint (https://proteinpaint.stjude.org/).

A recent study in mice determined that *Arhgef7* is essential for axon formation during cortical development (López Tobón et al., 2018). Complete knockouts of *Arhgef7* are embryonically lethal, therefore researchers generated a cortex-specific conditional knockout which facilitates the deletion in the dorsal telencephalon from E10.5 forward (López Tobón et al., 2018). In order to analyze the formation of axons in the developing mouse brain, sections from E17 *Arhgef7*-cKO embryos that were homozygous or heterozygous were stained with a neurofilament antibody (NF) and a nuclear marker (Hoechst 33342) (López Tobón et al., 2018). The immunostaining showed a loss of axons in the intermediate zone (IZ) and the hippocampus (López Tobón et al., 2018). These results indicate that *Arhgef7* is required for the formation of axons during both cortical and hippocampal development (López Tobón et al., 2018). Without *Arhgef7*, there is an extensive loss of axons (López Tobón et al., 2018).

The high expression of *ARHGEF7* in the brain, along with its role in axon formation and the reported mouse phenotype, make this gene a very exciting CMM candidate gene.

1.8 Rationale and Objectives

Samples were obtained from a large multigenerational family with unexplained CMM from Italy. These individuals were negative for variants in the known CMM genes (*DCC*, *RAD51*, *DNAL4*, and *NTN1*). Whole exome sequencing was performed and a heterozygous frameshift variant, c.1751_1752del, that leads to p.Asn584Thrfs*90 and that replaces the last 219 amino acids with 90 abnormal amino acids, was found in *ARHGEF7* (Gene ID: 8874) in all affected family members. Since this variant maps at least 50 nucleotides upstream of the last exon junction, it likely leads to a haploinsufficiency mechanism such as mRNA decay and loss of function of the encoded protein. Other possible mechanisms include dominant negative effects. *ARHGEF7*, also known as *βPIX* or *COOL1*, is a gene which encodes the Rho guanine nucleotide exchange factor 7, a member of the GIT-PIX complex, and plays a critical role in controlling cell polarity, adhesion, axonal guidance, and migration (Zhou et al., 2016).

Based on the genetic and functional data presented above, we hypothesize that *ARHGEF7* plays an important role in the pathogenesis of CMM in an affected family from our CMM cohort. Our overall goal is to validate the role of *ARHGEF7* in CMM pathogenesis using the zebrafish model. We expect that zebrafish *arhgef7* knockouts will exhibit CMM-like movements and abnormal decussation of the Mauthner hindbrain reticulospinal neurons.

Our objectives are: (1) To create a frameshift deletion at the corresponding site in the zebrafish orthologues using CRISPR-Cas9 technology, (2) To conduct overexpression assays of the wild-type and mutant *ARHGEF7*, (3) To conduct detailed phenotypic analyses of the mutant zebrafish.

Chapter II: Methods

2.1 Zebrafish Care

All zebrafish care procedures were carried out in accordance with the guidelines set out by the Canadian Council for Animal Care. Adult zebrafish were housed in tanks with water supplied by a recirculating system (28.5°C, pH 7-8, dissolved oxygen ≥87%) with ≥10% daily renewal. Aquaria water was made from distilled water and was supplemented to achieve the conditions above. Fish were fed twice with commercial flakes and once with live, adult Artemia each day. Zebrafish were kept on a 14:10 hour (light:dark) light cycle.

Sexually mature zebrafish were crossed for breeding beginning around 10-12 weeks. Females and males were separated in a breeding chamber inside of a tank designated for breeding the night prior to crossing. The following morning, the separator was removed, and breeding would commence. Eggs were collected, rinsed with embryo medium water, placed in petri dishes with approximately 50 eggs to a dish, and screened under the microscope to remove unfertilized or unhealthy eggs. Zebrafish embryos were raised in petri dishes filled with embryo medium water in an incubator at 28.5°C until 4dpf. Embryos were then placed in a tank with approximately 1L of water and were fed First Bites. Gradually, water levels were increased until 7dpf, the point after which the water was supplied by the recirculating system. Fish were raised until 3 months

All animal holding, breeding, and experimentation were performed in accordance with the CHU-Sainte Justine animal care policies and under an approved animal use protocol.

2.2 CRISPR-Cas9

There are 2 orthologues in zebrafish *arhgef7a* (Gene ID: 553493) and *arhgef7b* (Gene ID: 494081) of human *ARHGEF7* (Gene ID: 8874). Both orthologues have similar identity levels with the human protein (p=76.55% and p=74.56% respectively). We created a CRISPR-induced mutant at the corresponding site as the human patient mutation in both zebrafish orthologues *arhgef7a* and *arhgef7b* using the CRISPR-Cas9 technology (Figure 9) (Moreno-Mateos et al., 2015, Li et al., 2016).

In order to create the *arhgef7a* zebrafish mutant line, gRNA was designed using the online tool CRISPRscan (http://www.crisprscan.org/). Primers flanking the mutation site in exon 15 were designed to conduct PCR to detect the mutation introduction. Cas9 mRNA(100ng/ul) and gRNA(30ng/ul) were injected in embryos at the one-cell stage. The larvae were genotyped, and mosaicism was exhibited. These mosaic F0 fish were later crossed to wild type (WT) fish. These F1 fish were then raised to adults and genotyped. The heterozygous F1 fish were then crossed to result in F2. The F2 fish were genotyped, exhibiting a homozygous frameshift mutation at the corresponding location as the patient human mutation. The first generation of heterozygotes no longer produced fertilized eggs due to old age. Consequently, homozygous male fish were crossed to WT female fish to obtain the next generation of heterozygous fish.

In order to create the *arhgef7b* zebrafish mutant line, two gRNA were designed and were microinjected into zebrafish embryos.

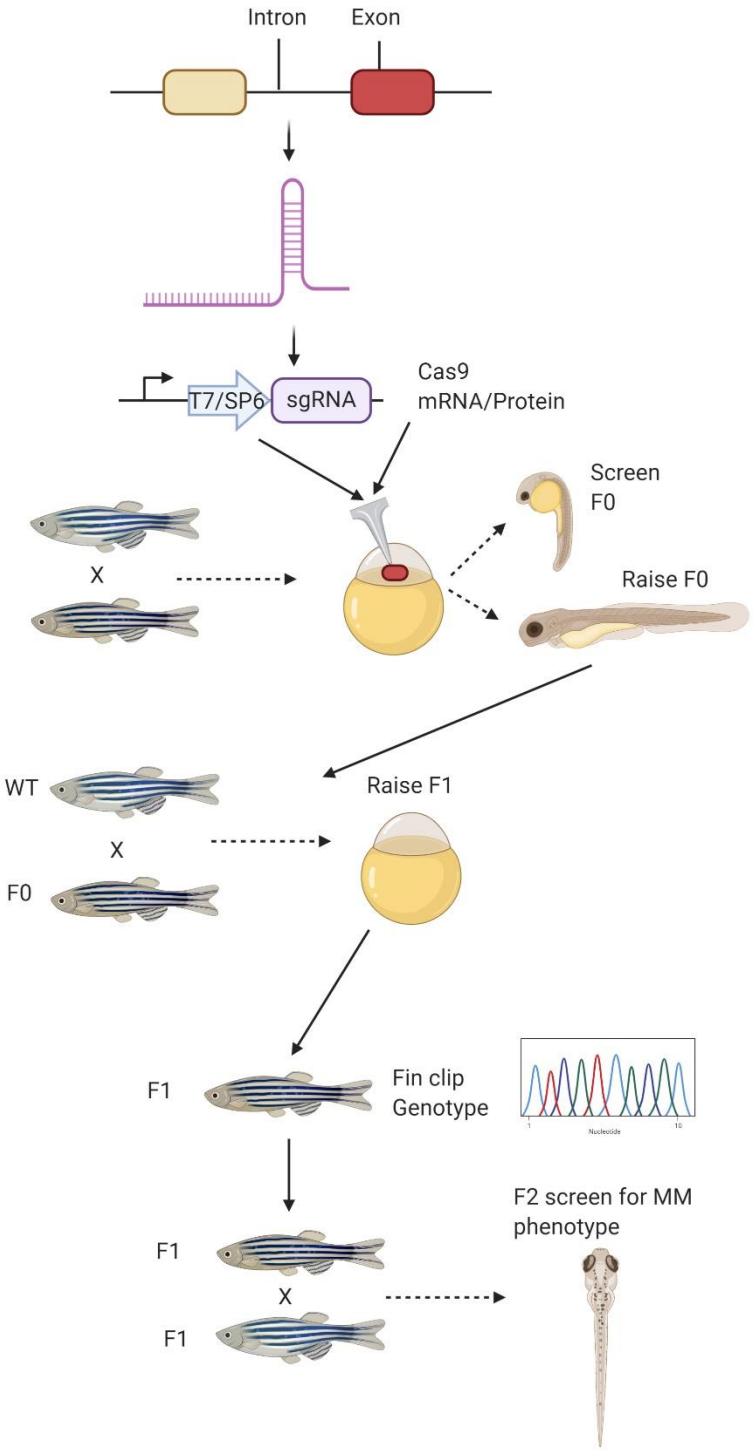

Figure 9. Schematic of CRISPR-Cas9 Methodology. Adapted from Li et al. (2016). Created with BioRender.com.

2.3 Zebrafish Genotyping

Zebrafish whole embryo genotyping was performed by adding 20 µL of 50mM NaOH was added to each well and DNA was extracted by boiling at 98°C for 10 minutes. Then, 5µL of 100mM pH 8.0 Tris HCl was added to buffer the pH. The PCR mixture consisted of 5µL Standard 5x buffer (New England Biolabs, USA), 0.5µL 10mM dNTPs, 0.5µL of each primer, 0.15µL OneTaq® DNA Polymerase (New England Biolabs, USA), 16.35µL ddH_2O, and 2µL of extracted DNA. The PCR conditions included 1 cycle for the initial denaturation at 94°C for 30 seconds, followed by 30 cycles of 94°C for 15 seconds, 50°C 15 seconds, 68°C for 30 seconds, and 1 cycle at 68°C for 5 minutes for the final extension, with a hold at 16°C. The PCR reactions were then electrophoresed on an agarose gel and sent for Sanger sequencing to Génome Québec (Montréal, QC, Canada).

For the genotyping of adult zebrafish, zebrafish were anesthetized with tricaine (3-amino benzoic acid ethyl ester also called ethyl 3-aminobenzoate). Then, the fins of the zebrafish were amputated, and the fish were returned to their respective tanks and were monitored for recovery. All other procedures regarding DNA extraction, PCR, and sequencing were the same as described above for embryo genotyping.

2.4 HRM Zebrafish Genotyping

Whole larvae were genotyped following the behavioral assays using the HotSHOT genomic DNA extraction technique followed by a high-resolution melting (HRM) assay (Samarut et al., 2016) (Figure 12). Larvae were anesthetized with one drop of tricaine, 20 µL of 50mM NaOH was added to each well, and DNA was extracted by boiling at 100°C for 10 minutes. 2.2 µL of 100mM pH 8.0 Tris HCl was then added to buffer the pH (Samarut et al., 2016). Then, the HRM PCR reaction was prepared by including 2.5 µL HRM dye, 1 µL ddH_2O, 0.25 µL Forward

primer, 0.25 µL Reverse primer, and 1 µL extracted gDNA (Samarut et al., 2016). The PCR conditions for HRM include 45 cycles of 10 seconds 95°C and 30 seconds at 60°C for amplification, followed by one cycle of 30 seconds at 95°C, 60 seconds at 60°C, 10 seconds at 95°C, then 10 seconds at 40°C for cooling (Samarut et al., 2016). After the HRM PCR, the melting peaks were analyzed to determine genotype of each sample in each well.

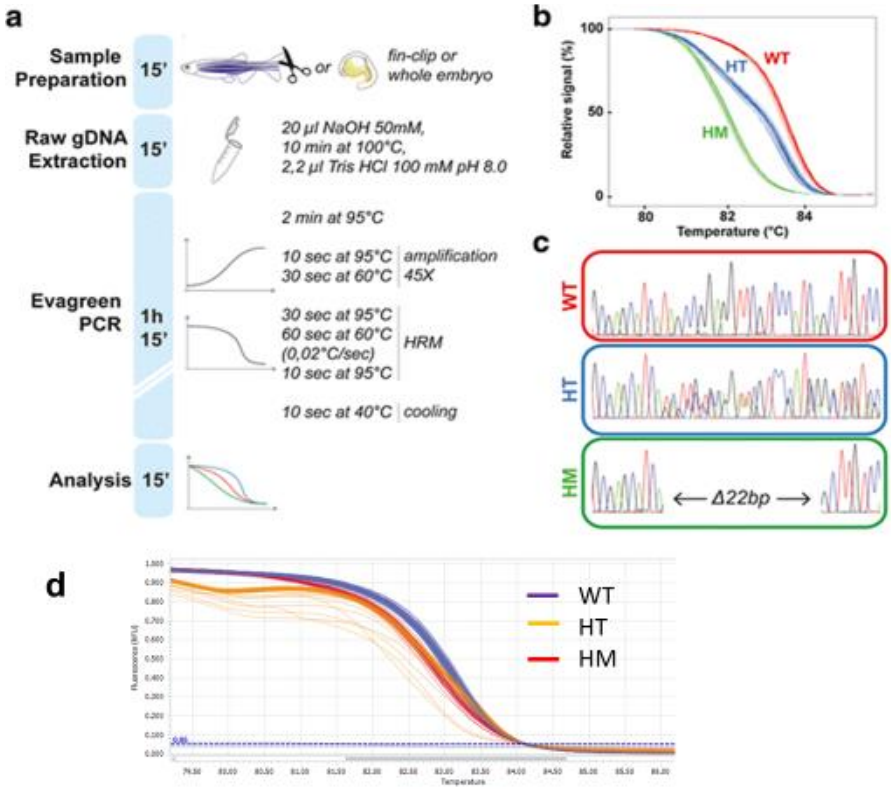

Figure 10. Overview of HRM-based Genotyping. A) To perform HRM-based genotyping, the fin of a zebrafish is cut or the whole embryo is used. Then, the gDNA is extracted and the Evagreen PCR is performed (Samarut et al., 2016). B and C) Afterwards, the melting profiles can be analyzed to determine the genotypes of the samples and sequencing can be used to confirm the genotype (Samarut et al., 2016). D) Example of an *arhgef7a* HRM-based genotyping result. A-C from Samarut et al. (2016) (Creative Commons Attribution 4.0 International License (http://creativecommons.org/licenses/by/4.0/).

2.5 RT-qPCR

We planned to perform quantitative real-time RT-PCR (RT-qPCR) to look for evidence of nonsense-mediated mRNA decay of *arhgef7a* and *arhgef7b* mutant mRNA, but we were unable to complete these experiments due to the COVID-19 laboratory shutdowns.

To do this, we planned to follow the Cold Spring Harbor Protocol for qRT-PCR of zebrafish transcripts (Lan et al., 2009). We planned to collect 20-50 embryos per line, use the TRIzol extraction method for euthanasia, wash the homogenization probe (2x DEPC-treated H_2O, 1x RNaseZap, 1x DEPC-treated H_2O), homogenize the sample for 30 seconds, incubate the sample on dry ice for 30 seconds, homogenize the sample for 30 seconds, incubate the sample for 5 minutes at room temperature, clean the probe (1x 75% ethanol, 1x DEPC-treated H_2O, 1x 75% ethanol, 1x DEPC-treated H_2O), isolate the RNA with TRIzol, purify the RNA, check the RNA concentration using the NanoDrop spectrophotometer, perform reverse transcription and prepare the cDNA, prepare reactions (1X Platinum SYBR Green qPCR SuperMix-UDG, 0.3 µM each of the forward and reverse primers, 2 µL of template RNA, 2 µL of diluted cDNA, RNase- and DNase-free H_2O to a final volume of 10 µL), perform RT-qPCR (40 amplification cycles, 15 sec at 95°C, followed by 1 min at 60°C), and analyze (Lan et al., 2009).

2.6 Cloning

In order to conduct overexpression assays, we first tried to utilize the Sequence and Ligation-Independent Cloning (SLIC) technique, which uses in vitro homologous recombination and single-strand annealing for the assembly of multiple DNA fragments in one reaction (Li & Elledge, 2007). We designed primers to be compatible with *ARHGEF7*, the SP6 promoter region, and to be cut by the BamHI enzyme. We amplified the *ARHGEF7* insert, prepared from human cDNA, using the Prime Star GXL DNA polymerase. We then purified the insert

containing *ARHGEF7* using the QIAquick PCR purification column (Qiagen). We digested the vector PCS2+ and purified it in solution. We then treated the vector and the insert separately with T4 DNA polymerase in 20 µL reactions for 30 minutes. We stopped the reactions by adding 2 µL volume of 10 mM dCTP. We used 150 ng of the vector and the appropriate amount of insert (90 ng) for the annealing reaction step, and we transformed 4 µL of the annealing mix into 950 µL of NEB cells and plated them on ampicillin plates. Colonies were picked and transferred to culture tubes to incubate overnight. BioBasic Mini Prep was performed to purify. Afterwards, the BioBasic Mini Prep DNA result was digested using XhoI, which cut inside the insert and vector, with bands at 1.2 and 5.3 kb respectively. However, this cloning experiment resulted in a gap in the sequence, where Exons 2 and 3 were missing.

After a series of failed attempts to re-introduce the missing exons using large primers and the SLIC method, a modified, alternative cloning method was employed to artificially introduce the missing exons (Figure 11). This method entailed using a series of "PCR on PCR" reactions. First, the original PCR of pCS2+-*ARHGEF7* (with the missing exons) was used as a template, then, R1 (GGTTACCAGATGCTGAGGAGGCTGGGAAGGAGGAAACAGGAGCTCCAGCCGCAGGGAAGC)/F2(AGGTCCTCAGTTCCTTAGTGACTCTAAATAAAGTAACAGCAGACATCGGGCTGGGGAGT) primers were used to amplify the region surrounding the missing exons, resulting in "PCR1".

The primer pair sequence for F3 (AGGTCCTCAGTTCCTTAGTGACTCTAAATAAAGTAACAGCAGACATCGGGCTGGGGAGT)/R3(AGTCACTAAGGAACTGAGGACCTTGTTAAAATTCTGCCCCTGATACAAATCATTTGCATC) was quite long (60bp each), resulting in the primers annealing to themselves

rather than to the template. Therefore, we used the “PCR 1” reaction as the template and annealed each primer separately. Furthermore, “PCR 1” was used as a template and F3 primer was used to regain part of the sequence of the missing exon, resulting in “PCR 2”.

Simultaneously, “PCR 1” was used as the template in a separate reaction with the R3 primer. Next, we combined 10uL of each “PCR 2” and “PCR 3”, digested this mixture with DPNI enzyme, heat inactivated the reaction, and denatured then reannealed the mixture. Finally, we transformed final PCR mixture in DH5α cells, picked 20 colonies, performed BioBasic Mini Prep, and digested the BioBasic Mini Prep DNA using SacI enzyme.

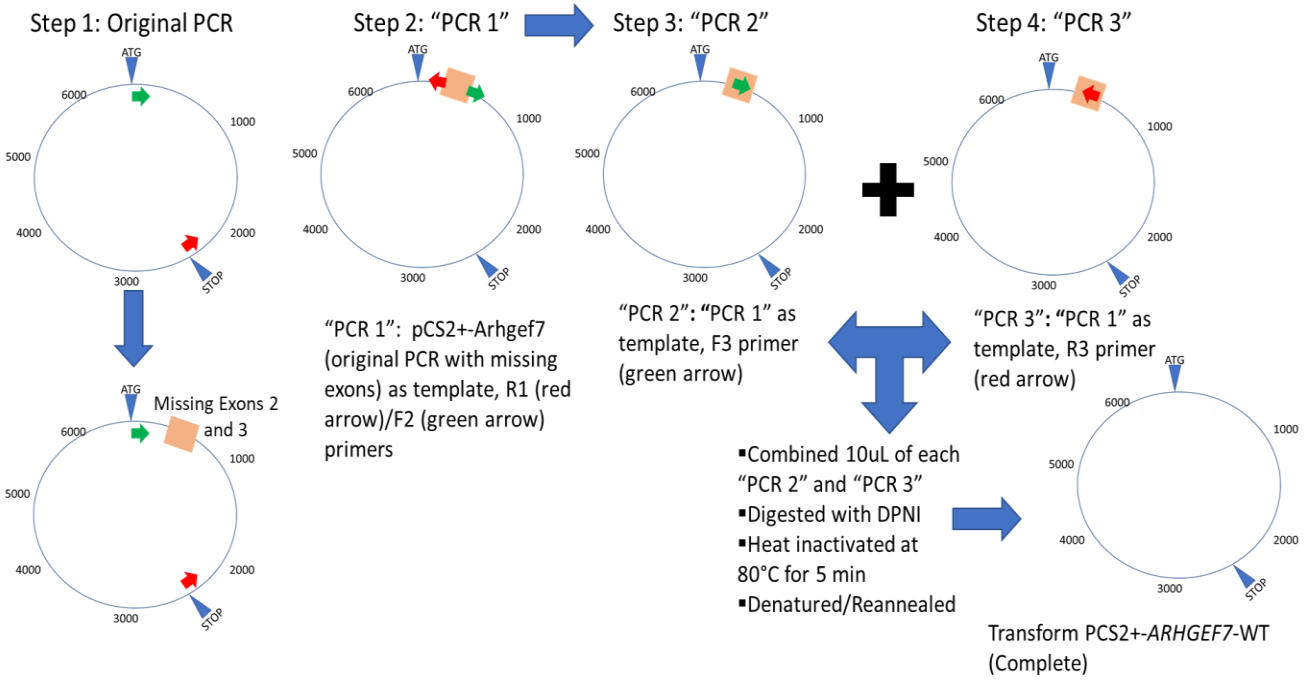

Figure 11. Design of alternative cloning method.

This resulted in two potential clones (named “FR1” and “FR5”), which we sent for sequencing. Using this alternative method, we successfully introduced the missing exons for the “FR1” clone, and we have the complete sequence of PCS2+-*ARHGEF7*-WT (Figure 12).

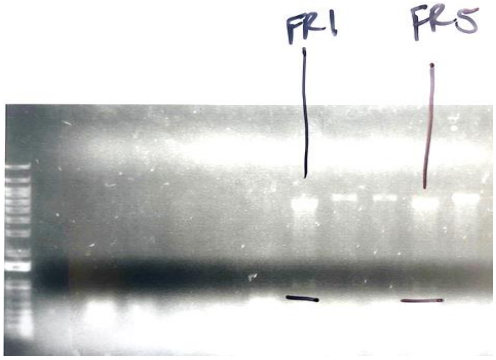

Figure 12. Cloning digestion result using SacI enzyme.

2.7 Mutagenesis

Following the cloning experiment, we began the site-directed mutagenesis protocol to introduce the AC deletion resulting in the p.Asn584Thrfs*90 mutation. *In vitro* site-directed mutagenesis is an important technique, used to characterize protein structure-function relationships and for carrying out vector modification (Stratagene, 2007). Stratagene’s QuikChange® XL Site-Directed Mutagenesis has a high efficiency at approximately 80% (Stratagene, 2007).

We performed temperature cycling using the PFU Ultra enzyme to have high efficiency, with no undesired mutations. Our mutation was contained within the mutagenesis primer pair (Arhgef7-ac-del-m-F: CGAAGGTCACGTTGGGAACCCACCATAAAGCCTCATT, Arhgef7-ac-del-m-R: AATGAGGCTTTATGGGTTCCCACAGACGTGACCTTCG). After the mutagenesis PCR, we had both the WT and the sequence with mutation. We then transformed the mutagenesis PCR in DH5α cells, picked 10 colonies from each plate, and performed Biobasic

Miniprep to obtain DNA. Six samples were sent for sequencing and 3 of the samples had the correct AC deletion mutation (Figure 13). The “D8” sample was used to prepare the RNA.

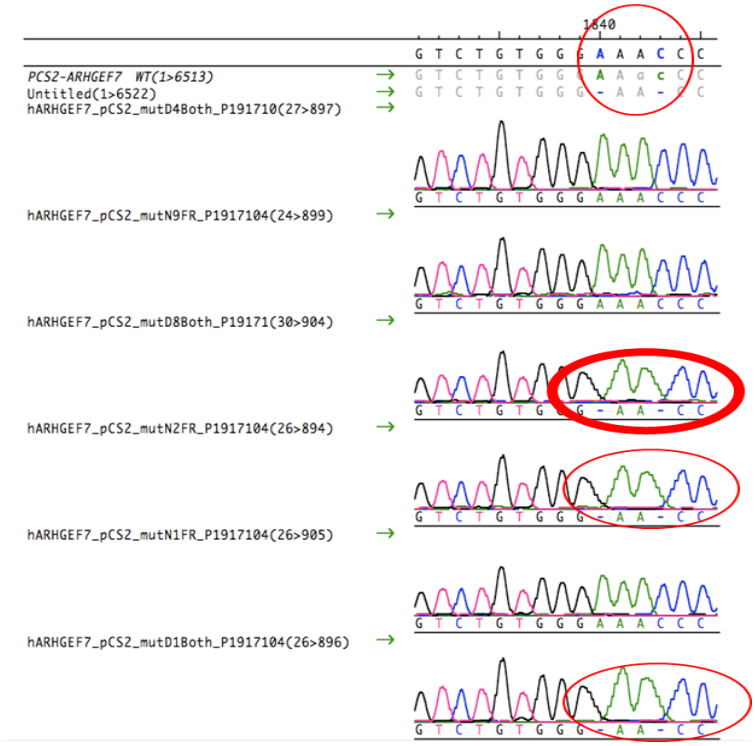

Figure 13. Mutagenesis chromatogram data. Sample circled in bold red (hARHGEF7_pCS2_mutD8Both_P1917) was used to prepare the RNA to be used for microinjection.

The BioBasic Miniprep DNA was digested with NOT I FD to linearize the plasmid DNA. Then, the DNA was purified with Qiaex II, and we followed the mMessage mMachine Procedure for High Yield Capped RNA Transcription (Figure 14). The RNA was stored at -80°C. We planned to conduct overexpression assays to further assess the effects of *ARHGEF7* in zebrafish, but we were unable to complete these experiments due to the COVID-19 laboratory shutdowns.

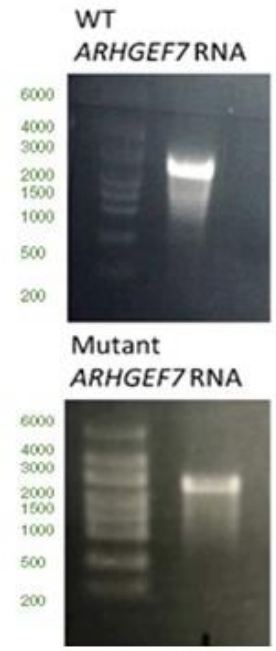

Figure 14. Gel pictures of WT and Mutant RNA.

2.8 Behavioral Assays

Behavioral analyses of both wild-type and mutant larvae were performed to assess mirror-like as previously described for zebrafish *dcc* mutants (Jain et al., 2014) (Figure 15). We examined swim patterns of wild-type and mutant larvae. This allowed us to determine whether rhythmic alternation between the left and right sides was altered. Precise movement deficits were examined by investigating the performance of wild-type and mutant larvae in response to light startle stimuli at millisecond resolution using a DanioVision device (Noldus, Wageningen, The Netherlands). The EthoVision XT package (Noldus) was used to analyze larval movement kinematics and turn angle.

The rotation parameter is useful for research on brain defects (Noldus, 2020). Rotations are based on the turn angle, and turn angle represents a change in the direction of movement. Therefore, clockwise and counterclockwise rotation frequencies were calculated using the EthoVision XT software.

Other parameters of interest include turn angle and angular velocity. The turn angle represents a change in the direction of movement. During an escape or startle response, the fish responds to a startling stimulus by presenting a large body angular acceleration and displacement (Kalueff et al., 2013). The first stage of a startle response is a ‘C-bend’ of the fish body (C-start) and a contralateral bend follows (Kalueff et al., 2013). In larval zebrafish, startle responses involve fast turning and subsequent burst swimming (Kalueff et al., 2013).

Blind genotyping was performed using the HRM assay immediately after each behavioral experiment trial (Samarut et al., 2016).

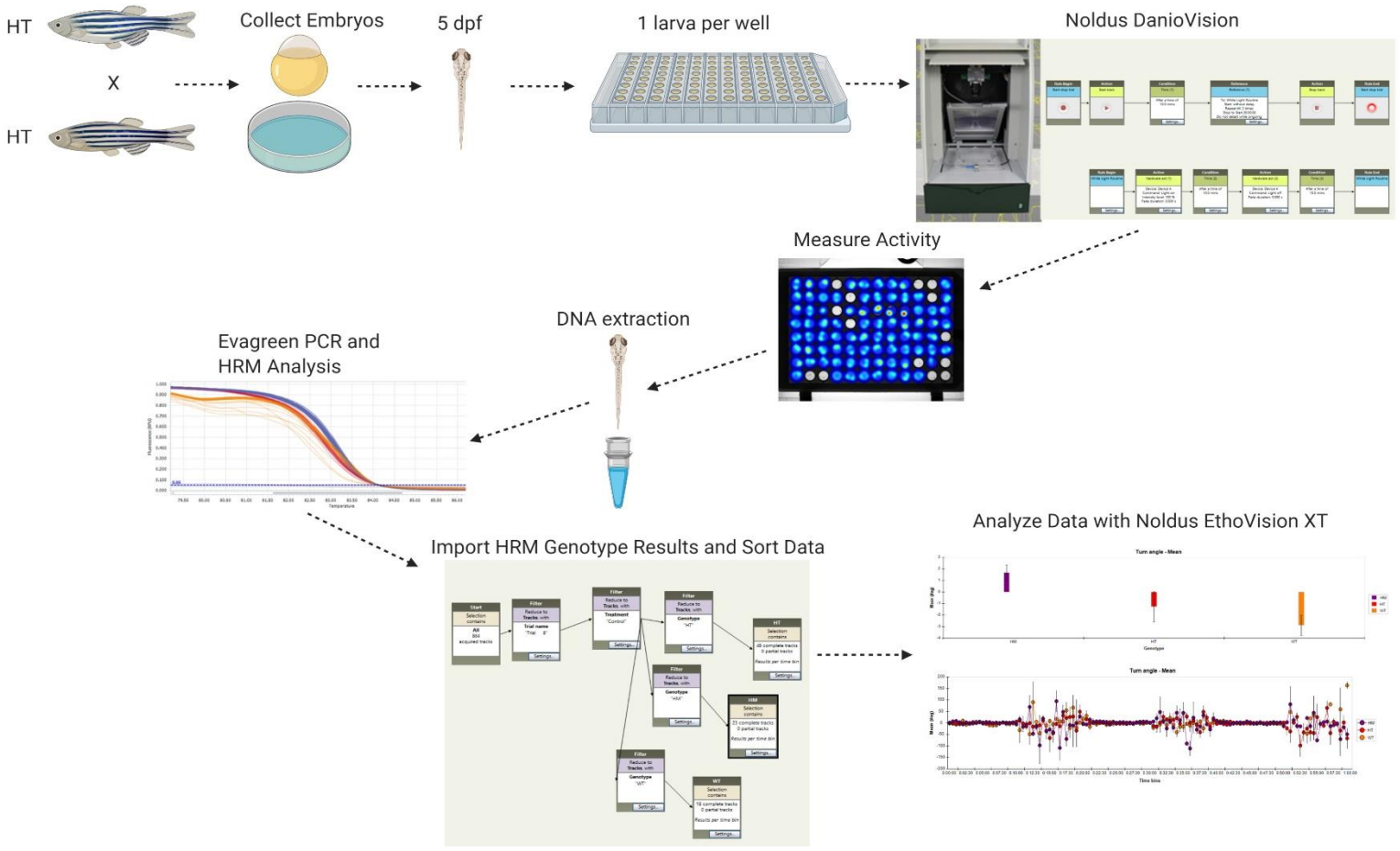

Figure 15. Schematic of Behavioral Experiment Methods. Heterozygous (HTZ) females were crossed to heterozygous males. The embryos were collected and screened. At 5 dpf, larvae were transported to the CR-CHUM for behavioral testing. Alternating light-induced startle response trials were the most used experimental condition, where fish were subjected to a white light routine comprised of 10-minute bouts of alternating the light off and on. Activity was measured blind to genotype by the Noldus DanioVision. Following the completion of the trial, larvae were anesthetized, DNA was extracted, and the Evagreen PCR and HRM analysis was performed. The HRM genotyping results were imported into the EthoVision XT software and the activity data were analyzed. Image of Noldus DanioVision machine from https://www.noldus.com/daniovision. Created with BioRender.com.

2.9 Immunohistochemistry

dcc mutants exhibited defects in the commissural trajectories of the Mauthner hindbrain array (Jain et al., 2014). This area of the brain is known to participate in escape behavior induced by light, sound, or touch (Colwill and Creton, 2012). To see if there are similar defects with *arhgef7* mutants, we aimed to blindly examine 3-5 *arhgef7a* and *arhgef7b* mutant embryos, using immunostaining with the anti-neurofilament M antibody αRMO44, an antibody that recognizes the identifiable primary reticulospinal neurons of zebrafish. Jain et al. (2014) examined 60–72 hours post fertilization (hpf) embryos for hindbrain reticulospinal immunofluorescence by raising the embryos in 0.2 mm phenylthiourea/E3 from 24 hpf to prevent pigmentation, fixing the embryos with 2% trichloroacetic acid/PBS, and staining the embryos with anti-intermediate neurofilament M (αRMO44).

We began the immunostaining for WT embryos following an adapted protocol from Santos et al. (2018). WT fish were crossed and were raised in 0.2 mm phenylthiourea/E3 (PTU) from 24 hpf to prevent pigmentation. The embryos pretreated with 2mg/mL pronase at 28°C for 30 mins. The embryos were washed with PBS (1x) for 5 min x 3. Then, the embryos were fixed at 72hpf in either 2% trichloroacetic acid/PBS for 3 hours at RT or 4% PFA at RT for 1 hour. Afterwards, the embryos were washed with PBS (1x) for 5 min x 3. The embryos were then dehydrated with a MeOH/PBS graded series (25%, 50%, 75%, 100%) for 5 mins in each solution. The embryos were transferred to fresh 100% MeOH and stored at -20 overnight. The embryos were then rehydrated with a MeOH/PBS graded series (75%, 50%, 25%) for 5 mins in each solution. Then, the embryos were digested with Proteinase K (0.5uL for 30 min) at RT, rinsed in PBS, and post-fixed with either 4% PFA or 2% trichloroacetic acid/PBS for 25 mins at RT. The embryos were washed with PBS/Triton-X for 5 mins x 3 and blocked with IB blocking

buffer (0.1 m phosphate buffer/0.2% BSA/0.5% Triton-X/2% normal goat serum) for 1 RT then overnight at 4°C. Then, 500uL of IB block was removed, and we added 5uL αRMO44 primary antibody (1:100) (ThermoFisher Scientific). The primary antibody was incubated at RT for 1 hour then overnight at 4°C. The embryos were washed with PBS for 15 min x 4. Then, a dilution for the secondary antibody Alexa-555-goat-anti-mouse (1:250) was prepared in IB blocking buffer. The covered embryos incubated in the secondary antibody solution for 2 hours at RT. Then, they were washed with PBS for 20 min x 4, washed with PBS for 5 min x 3, washed with Glycerol/PBS graded series for 20 mins in each solution, stored in 50% Glycerol at 4 °C, and were examined under the microscope. We planned to repeat this IHC method for *arhgef7a* and *arhgef7b* mutants. However, all laboratory experiments were halted due to COVID-19.

2.10 Statistical Analyses

Due to the Mendelian inheritance of *arhgef7a* and *arhgef7b*, each trial of approximately 96 larvae would consist of approximately 48 heterozygotes, 24 homozygotes, and 24 WT fish. There were also some HRM results that were unclear, where the HRM was negative or the genotype was unknown, and those samples would be excluded from the trial. Since each group of larvae for each trial were raised in separate petri dishes, the data was not pooled. Additionally, the inherently smaller sample sizes of the homozygotes and WT larvae prevented the use of parametric tests.

Statistical comparison of behaviors between groups was performed with GraphPad Prism v8.4.2 software. The Kruskal–Wallis *H* test by ranks, or one-way ANOVA on ranks, was used for the behavioral statistical analyses. This is a non-parametric test used for comparing three or more unmatched independent samples of equal or different sample sizes (McDonald, 2014). The Dunn's Multiple Comparison post hoc test was used to make comparisons between genotype groups. For this test, the null hypothesis is that there is no difference between groups, and the alternate hypothesis is that there is a difference between groups. Outliers were removed, as identified by GraphPad Prism 8.4.2's ROUT test for definitive outliers (Q=0.1%).

Chapter III: Results

3.1 Creation of Zebrafish *arhgef7* mutants by CRISPR-Cas9

There are two orthologues in zebrafish, *arhgef7a* (Gene ID: 553493) and *arhgef7b* (Gene ID: 494081), of human *ARHGEF7* (Gene ID: 8874). Both orthologues have similar identity levels with the human protein (p=76.55% and p=74.56% respectively). Zebrafish *arhgef7a* has been previously implicated in regulating Rho protein signal transduction and intracellular signal transduction (Tay et al., 2010). Zebrafish *arhgef7b* has previously been shown to be widely expressed throughout the brain and has been implicated in blood vessel development and angiogenesis, as well as vascular stabilization (Liu et al., 2007). Moreover, *arhgef7b* (βPix-A) splice site mutations have been shown to lead to hydrocephalus and severe cranial hemorrhage in zebrafish models (Liu et al., 2007).

The region where the human mutation is located is conserved at the nucleotide level for *arhgef7a* and *arhgef7b*. We introduced the human *ARHGEF7* mutation (NM_001113511.1: c.1751_1752delAC) in both zebrafish orthologues.

For the *arhgef7a* zebrafish mutant line (NM_001123235.1: c. 1701_1702delAC), mosaic *arhgef7a* F0 fish were later crossed to wild type (WT) fish, and heterozygous frameshift mutants were obtained. These F1 fish were then raised to adults and genotyped (Figure 16).

For the *arhgef7b* zebrafish mutant line (NM_001008624.1: c. 1807_1808delAC), two gRNA were designed and were microinjected into zebrafish embryos. Both gRNA worked with a low efficiency. After crossing the F0 fish to WT, heterozygous frameshift mutants were obtained (Figure 17).

There were no visible physical deformities in all *arhgef7a* and *arhgef7b* lines.

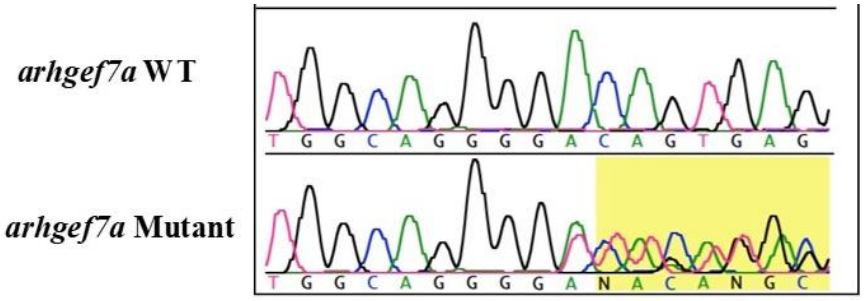

Figure 16. Chromatogram Data from arhgef7a F1 Zebrafish Generation. The beginning of the mutation sequence is highlighted in yellow, showing the heterozygous 11 nucleotide deletion resulting in a frameshift mutation.

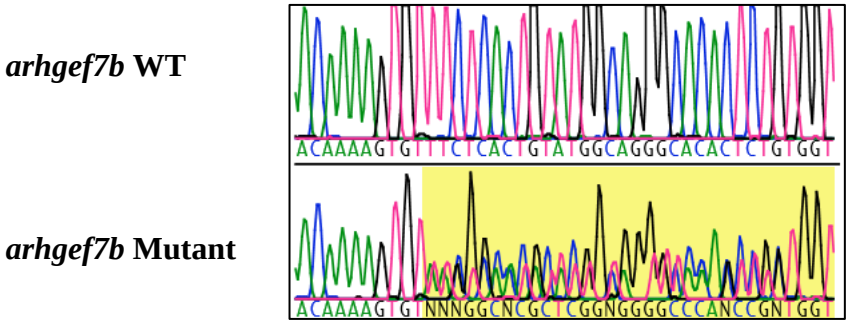

Figure 17. Chromatogram Data from arhgef7b F1 Zebrafish Generation. The beginning of the mutation sequence is highlighted in yellow, showing the heterozygous 14 nucleotide deletion resulting in a frameshift mutation.

3.2 Behavioral Assays

For the first behavioral testing run, homozygous *arhgef7a* fish were crossed to WT fish. However, we wanted to have all three genotypes, so the experiment was repeated using heterozygous *arhgef7a* mutant fish crossed to heterozygous *arhgef7a* mutant fish. For the second testing run, heterozygous *arhgef7a*-KO fish were crossed, transported to the CR-CHUM at 5dpf, and were subjected to a 16-hour light-induced startle response experimental trial to assess baseline behavior (Figure 18).

Homozygous fish exhibited higher rotation frequencies in both the clockwise and counterclockwise conditions around the one-hour mark. Because the results of the 16-hour light-induced startle response experimental trial indicated higher activity in homozygotes within the first hour, this time point was used for all trials thereafter.

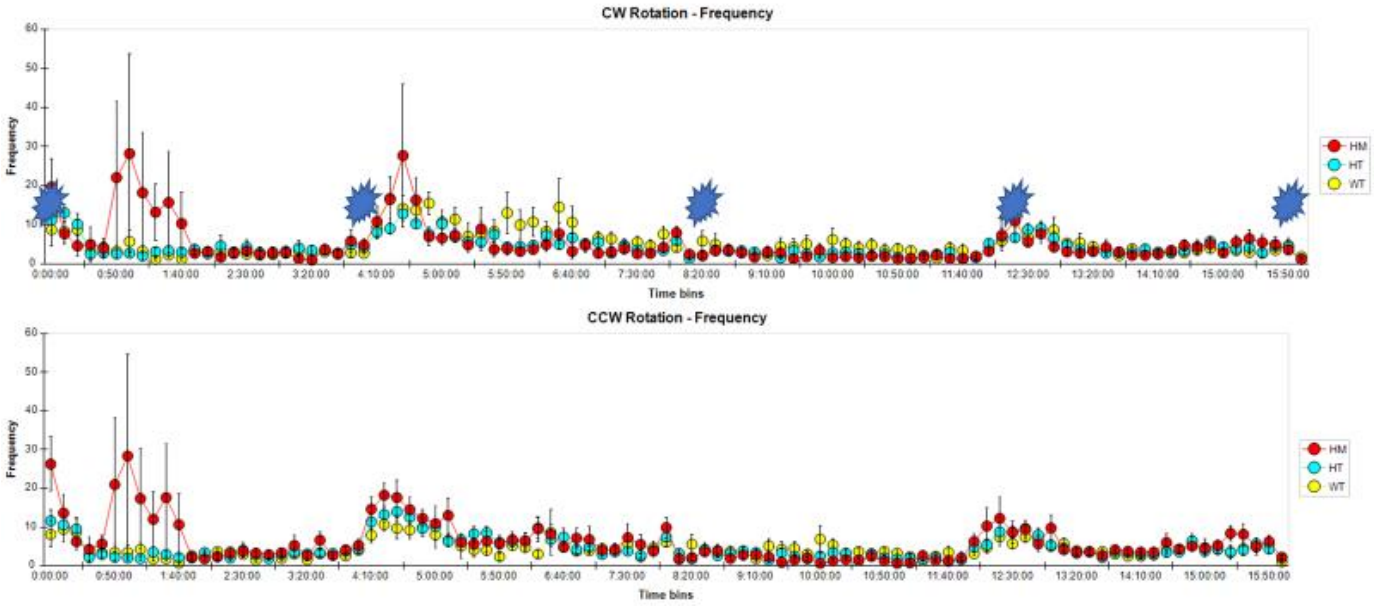

Figure 18. Clockwise and Counterclockwise Rotation Frequencies 16-Hour Trial. Homozygotes (HMZ) shown in red. Heterozygotes (HTZ) shown in blue. Wild-type (WT) shown in yellow. Blue stars in the top panel indicate time points when light is turned on and flashed off instantaneously.

3.2.1 *arhgef7a*

After the initial baseline assessment, three additional trials were conducted to assess startle responses of *arhgef7a* heterozygous intercrosses. Across the three trials, 288 larvae were tested. There were 96 fish included in Trial 1. The HRM results indicated that there were 21 homozygous (HM) fish, 42 heterozygous (HT) fish, 19 wild-type (WT) fish, and 14 fish were HRM negative or unknown. A Kruskal-Wallis H test showed that there was an overall statistically significant difference in turn angle between the different genotypes, H=27.15 (p = <0.0001) (Figure 19). A Dunn's multiple comparisons post hoc test revealed mean rank differences between groups. There was a significant difference in the HM vs. HT group comparison (37.19, p=0.0045) and the HM vs. WT comparison (60.03, p=<0.0001). However, there was no significant mean rank difference for the HT vs. WT group comparison (22.84, p=0.0060).

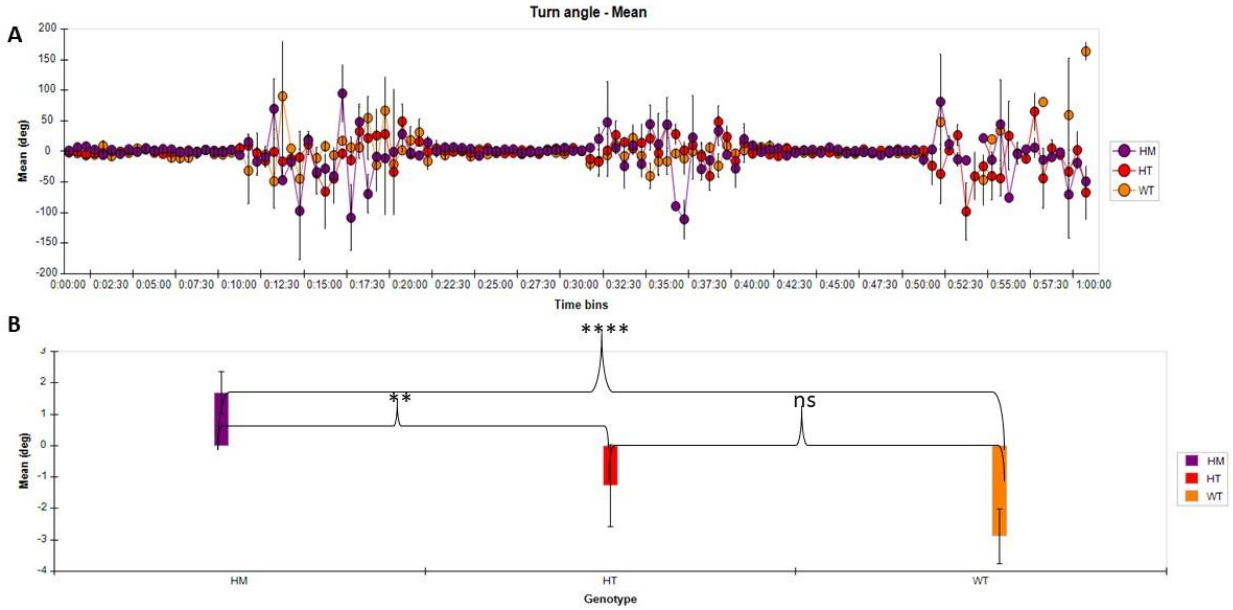

Figure 19. Relative Turn Angle Means for *arhgef7a* Larvae Trial 1. Homozygotes (HM) shown in purple (n=21). Heterozygotes (HT) shown in red (n=42). Wild-type (WT) shown in orange (n=19). A) Turn angle means by genotype represented over time with each point signifying the sum of activity in a 30s time bin. B) Overall turn angle means by genotype. Kruskal-Wallis H test revealed statistically significant difference in turn angle between the different genotypes, H=27.15 (p = <0.0001) (ns=p > 0.05, * = p ≤ 0.05 , **=p ≤ 0.01, ***=p ≤ 0.001, ****=p ≤ 0.0001).

Similarly, a Kruskal-Wallis H test showed that there was a statistically significant difference in angular velocity between the different genotypes, H=27.62, p = <0.0001 (Figure 20). A Dunn's multiple comparisons post hoc test revealed mean rank differences between groups. There was no significant difference in the HM vs. HT group. However, there was a significant mean rank difference between the HM vs. WT (-55.75, p=<0.0001) and HT vs. WT groups (-31.79, p=0.0060).

There were no observed differences in distance moved or maximum accelaration (Figures 21-22).

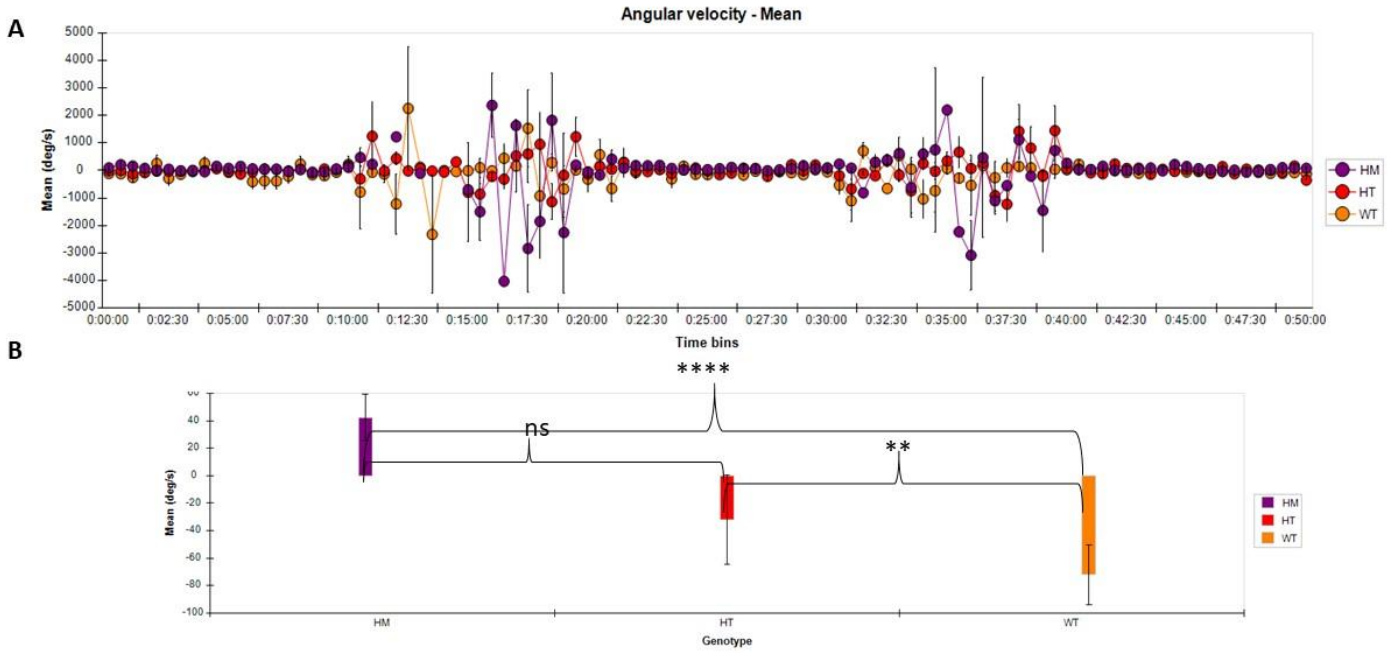

Figure 20. Relative Angular Velocity Means for *arhgef7a* Larvae Trial 1. Homozygotes (HM) shown in purple. Heterozygotes (HT) shown in red. Wild-type (WT) shown in orange. A) Overall angular velocity means by genotype. B) Angular velocity means by genotype represented over time with each point signifying the sum of activity in a 30s time bin. Kruskal-Wallis H test revealed a statistically significant difference in angular velocity between the different genotypes, H=27.62 (p = <0.0001) (ns=p > 0.05, * = p ≤ 0.05 , **=p ≤ 0.01, ***=p ≤ 0.001, ****=p ≤ 0.0001).

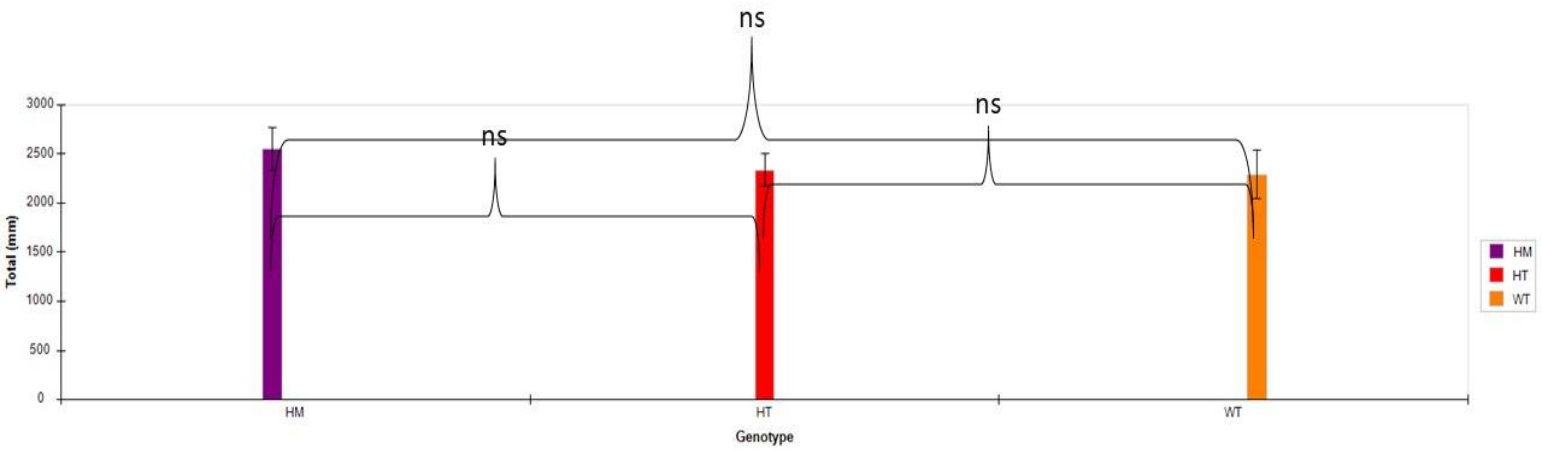

Figure 21. Mean Total Distance Moved (mm) for *arhgef7a* Larvae Trial 1. Homozygotes (HM) shown in purple. Heterozygotes (HT) shown in red. Wild-type (WT) shown in orange. Kruskal-Wallis H test revealed no overall significant difference (*H*=0.5024, p = 0.7779), (ns=p > 0.05).

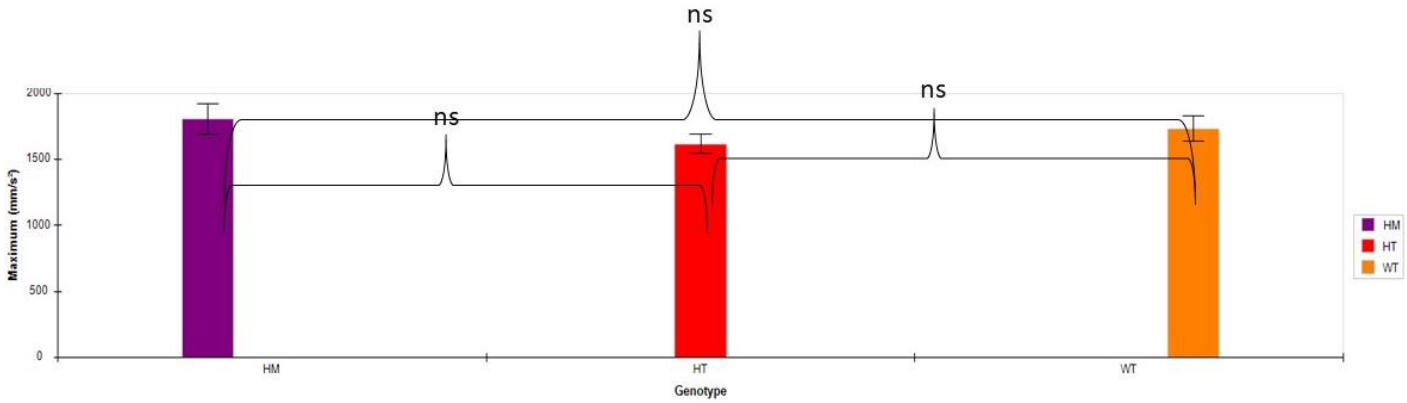

Figure 22. Mean Maximum Accelaration (mm/s^2) for *arhgef7a* Larvae Trial 1. Homozygotes (HM) shown in purple. Heterozygotes (HT) shown in red. Wild-type (WT) shown in orange. Kruskal-Wallis H test revealed no overall significant difference (*H*=0.9340, p = 0.6269) (ns=p > 0.05).

Trial 2 revealed a similar general pattern. There were 96 fish included in Trial 2. The HRM results indicated that there were 20 homozygous (HM) fish, 48 heterzygous (HT) fish, 12 wild-type (WT) fish, and 16 fish were HRM negative or unknown. A Kruskal-Wallis H test showed that there was a statistically significant difference in turn angle between the different genotypes, H=9.297 (p = 0.0096) (Figure 23). A Dunn's multiple comparisons post hoc test revealed mean rank differences between certain groups. There was a significant difference in the HM vs. HT group comparison (-34.12, p=0.0092). However, there was no significant mean rank difference for the HM vs. WT comparison (-24.84, p=0. 0976) and HT vs. WT group comparison (9.279, p=>0.9999).

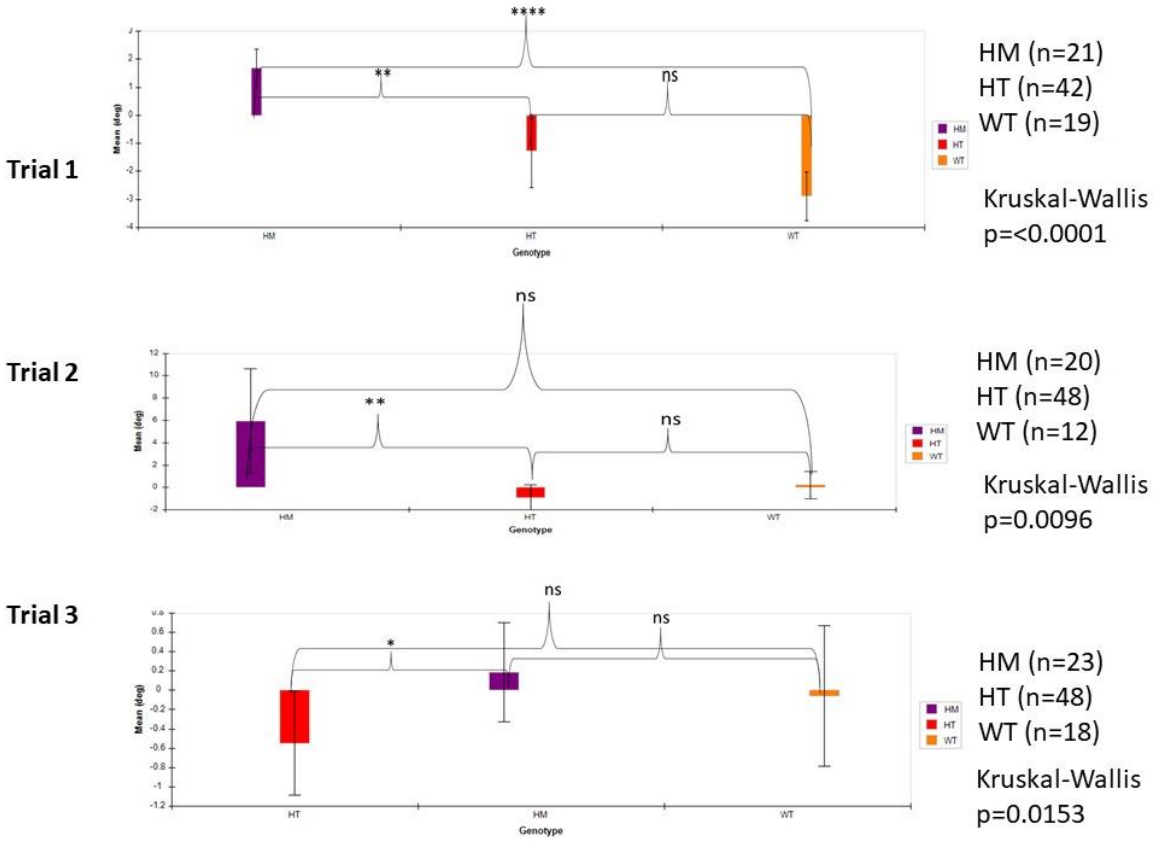

Figure 23. Relative Turn Angle Means for *arhgef7a* Larvae Trials 1-3. Homozygotes (HM) shown in purple. Heterozygotes (HT) shown in red. Wild-type (WT) shown in orange. Overall turn angle means by genotype. Kruskal-Wallis H test revealed statistically significant difference in turn angle overall between the different genotypes, (ns=$p > 0.05$, * = $p \leq 0.05$, **=$p \leq 0.01$, ***=$p \leq 0.001$, ****=$p \leq 0.0001$).

Trial 3 revealed a similar pattern. There were 96 fish included in Trial 3. The HRM results indicated that there were 23 homozygous (HM) fish, 48 heterzygous (HT) fish, 18 wild-type (WT) fish, and 7 fish were HRM negative or unknown. A Kruskal-Wallis H test showed that there was an overall statistically significant difference in turn angle between the different genotypes, H=8.364 (p=0.0153) (Figure 23). A Dunn's multiple comparisons post hoc test revealed mean rank differences between certain groups. There was a significant difference in the HM vs. HT group comparison (-33.38, p=0.0117). Yet, there was no significant mean rank difference for the HM vs. WT comparison (-19.15, p=0.2994) and HT vs. WT group comparison (14.23, p=0.6437).

When comparing absolute turn angle between the trials for only periods when the light was on and flashed off instantaneously, a Kruskal-Wallis H test showed that there was an overall statistically significant difference in turn angle between the different genotypes across all trials (Trial 1: p=<0.0001, Trial 2: p=0.0013, Trial 3: p=0.0078) (Figure 24). A Dunn's multiple comparisons post hoc test revealed mean rank differences between the HM vs. WT group comparison for all three trials (Trial 1: p=<0.0001, Trial 2: p=0.0065, Trial 3: p=0.0063). There was a significant mean rank difference for the HT vs. WT (0.0189) comparison for Trial 1 and HM vs. HT comparison for Trial 2 (p=0.0034). Yet, there was no significant mean rank difference for the HM vs. HT comparison for trials 1 and 3 and HT vs. WT group comparison for trials 2 and 3.

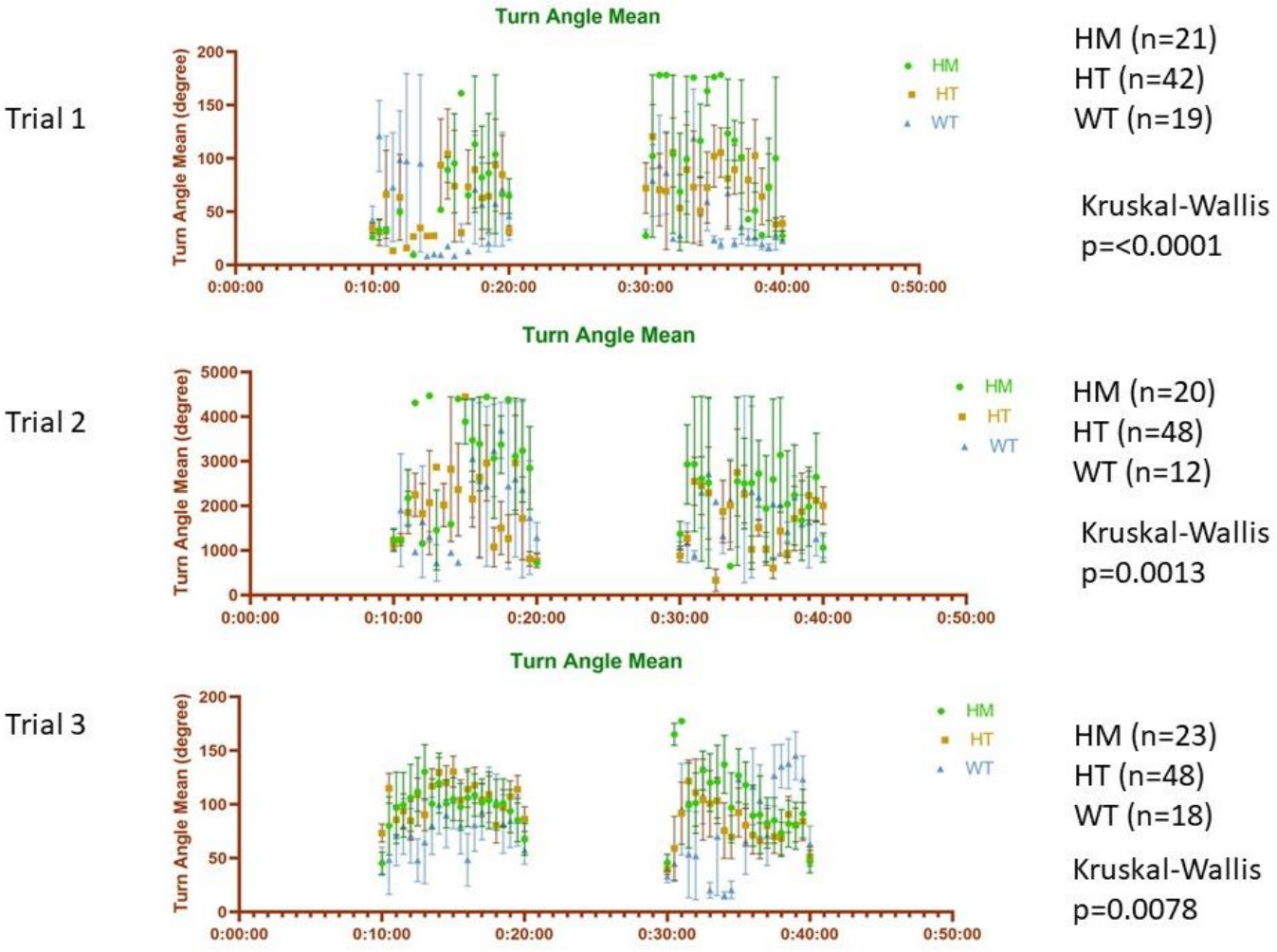

Figure 24. Absolute Turn Angle Means for *arhgef7a* Larvae Trials 1-3. Homozygotes (HM) shown in green. Heterozygotes (HT) shown in orange. Wild-type (WT) shown in blue. Turn angle means by genotype during periods when the light was turned on and flashed off instantaneously. Kruskal-Wallis H test revealed statistically significant difference in turn angle overall between the different genotypes across all three trials (Trial 1: p=<0.0001, Trial 2: p=0.0013, Trial 3: p=0.0078).

Additionally, there were observed differences in the frequencies of clockwise and counterclockwise rotations between the groups for Trial 3. A Kruskal-Wallis H test indicated that there was an overall statistically significant difference in clockwise (CW) (H=28.97 (p=<0.0001)) and counterclockwise (CCW) (H=22.68 (p=<0.0001)) turns between the different genotypes (Figures 25 and 26). Dunn's multiple comparisons post hoc tests revealed mean rank differences between certain groups for both directions. There was a significant difference in the HM vs. HT group comparison (CW: -46.63, p=0.0002; CCW: -33.26, p=0.0140) and the HT vs. WT group comparison (CW:58.08, p=<0.0001; CCW: 53.27, p=<0.0001). Yet, there was no significant mean rank difference for the HM vs. WT group comparison for either direction (CW:11.46, p=0.9278; CCW:20.01, p=0.2240).

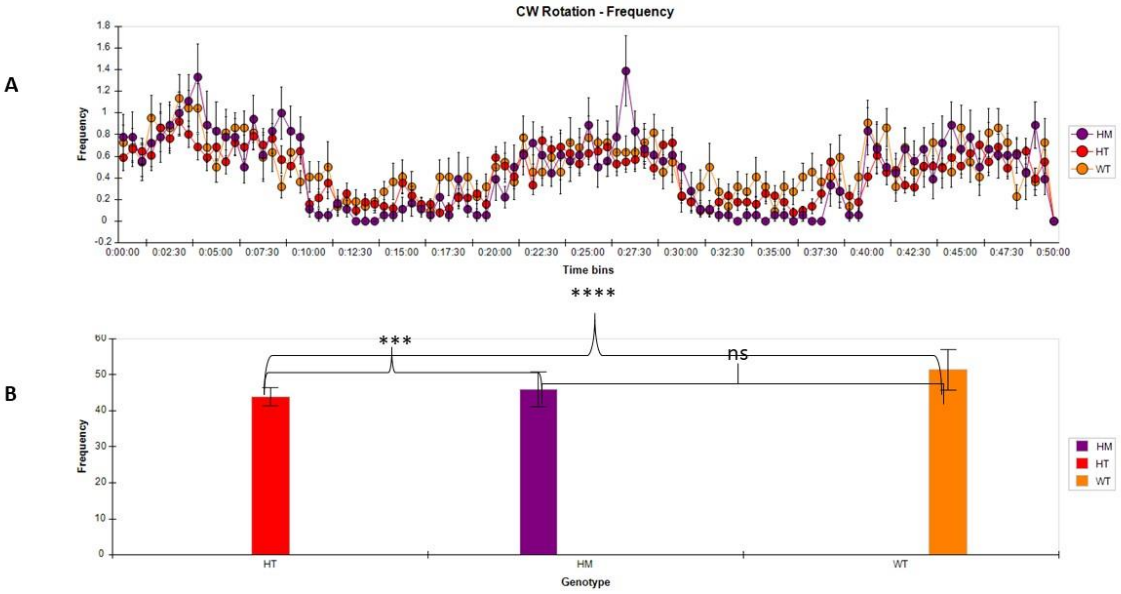

Figure 25. Overall Clockwise (CW) rotation frequencies for *arhgef7a* Larvae Trial 3. Homozygotes (HM) shown in purple. Heterozygotes (HT) shown in red. Wild-type (WT) shown in orange. A) Clockwise rotation frequencies by genotype represented over time with each point signifying the sum of activity in a 30s time bin. B) Overall clockwise rotation frequencies by genotype. Kruskal-Wallis H test revealed statistically significant difference in rotation frequencies overall between the different genotypes, H=28.97 (p=<0.0001) (ns=p > 0.05, * = p ≤ 0.05 , **=p ≤ 0.01, ***=p ≤ 0.001, ****=p ≤ 0.0001).

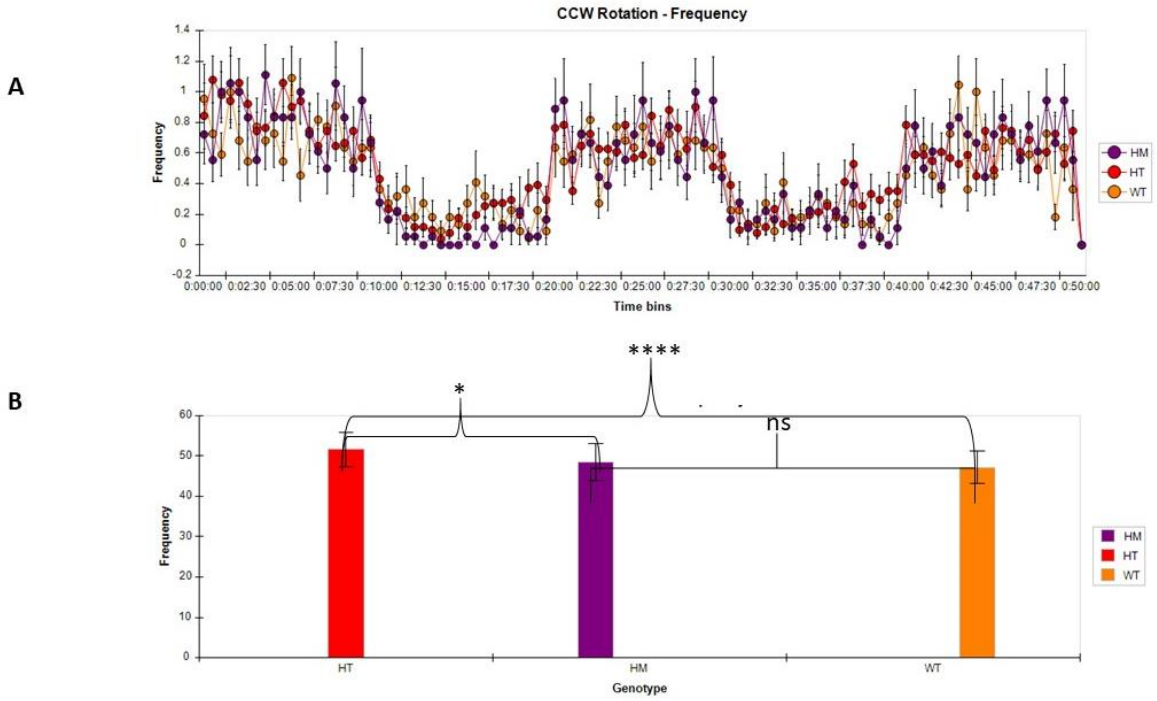

Figure 26. Overall Counterclockwise (CCW) rotation frequencies for *arhgef7a* Larvae Trial 3. Homozygotes (HM) shown in purple. Heterozygotes (HT) shown in red. Wild-type (WT) shown in orange. A) Counterclockwise rotation frequencies by genotype represented over time with each point signifying the sum of activity in a 30s time bin B). Overall clockwise rotation frequencies by genotype. Kruskal-Wallis H test revealed statistically significant difference in rotation frequencies overall between the different genotypes, H=22.68 (p=<0.0001) (ns=p > 0.05, * = p ≤ 0.05 , **=p ≤ 0.01, ***=p ≤ 0.001, ****=p ≤ 0.0001).

3.2.2 *arhgef7b*

Three trials were conducted to assess startle responses of *arhgef7b* heterozygous intercrosses. Across the three trials, there 251 larvae tested. There were 96 fish included in Trial 1. The HRM results indicated that there were 23 homozygous (HM) fish, 36 heterozygous (HT) fish, 18 wild-type (WT) fish, and 19 fish were HRM negative or unknown. A Kruskal-Wallis H test showed that there was an overall statistically significant difference in turn angle between the different genotypes, H=11.88 (p = 0.0026) (Figure 27). A Dunn's multiple comparisons post hoc test revealed mean rank differences between one set of groups. There was a significant difference in the HM vs. WT group comparison (42.15, p=0.0017). However, there was no significant mean rank difference for the HM vs. HT (19.52, p=0.3240) and HT vs. WT group comparisons (22.63, p=0.1932).

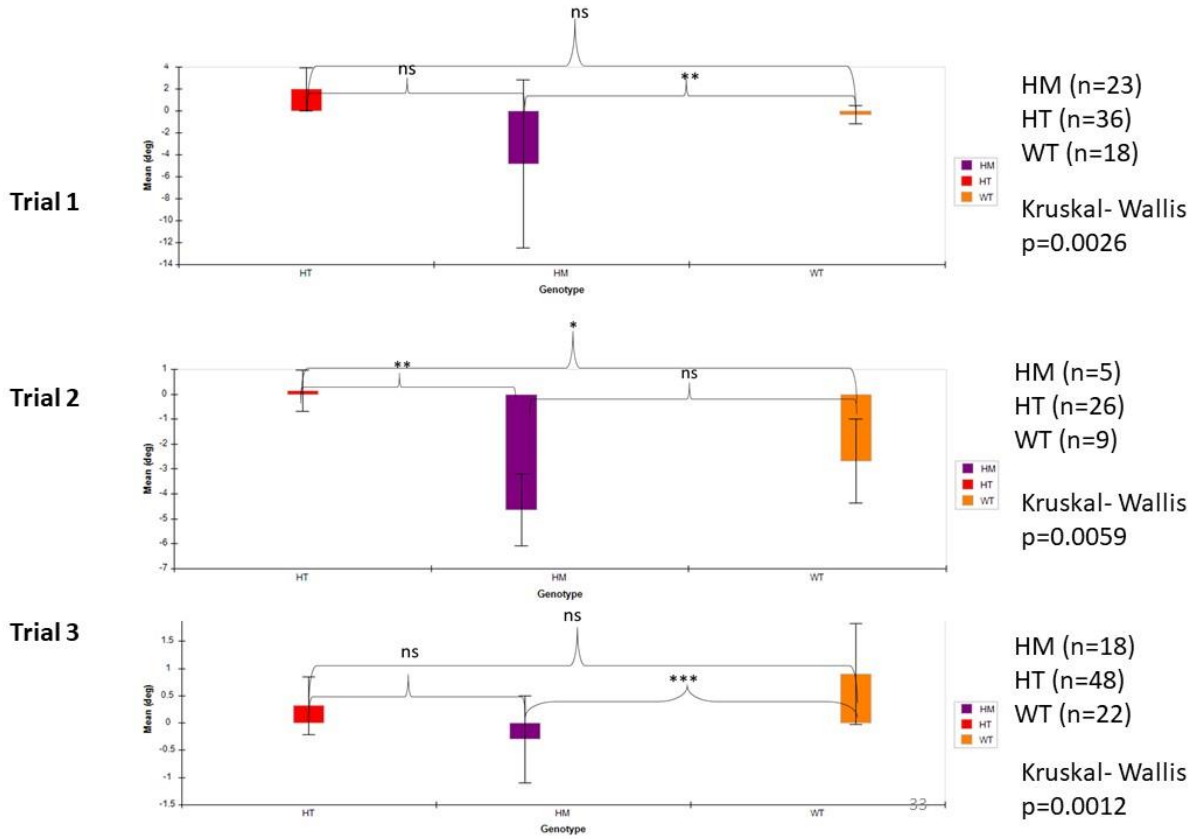

Figure 27. Relative Turn Angle Means for *arhgef7b* Larvae Trials 1-3. Homozygotes (HM) shown in purple. Heterozygotes (HT) shown in red. Wild-type (WT) shown in orange. A) Turn angle means by genotype represented over time with each point signifying the sum of activity in a 30s time bin. B) Overall turn angle means by genotype. Kruskal-Wallis H test revealed statistically significant difference in turn angle overall between the different genotypes (ns=$p > 0.05$, * = $p \leq 0.05$, **=$p \leq 0.01$, ***=$p \leq 0.001$, ****=$p \leq 0.0001$).

Trial 2 only included 59 larvae. The HRM results revealed that there were 5 homozygous (HM) fish, 26 heterzygous (HT) fish, 9 wild-type (WT) fish, and 19 fish were HRM negative or unknown. A Kruskal-Wallis H test demonstrated that there was an overall statistically significant difference in turn angle between the different genotypes, H=10.95 (p = 0.0042) (Figure 27). A Dunn's multiple comparisons post hoc test revealed mean rank differences between two set of groups. There was a significant difference in the HM vs. HT group comparison (-35.51, p=0.0075) and the HT vs. WT group comparisons (31.18, p=0.0237). However, there was no significant mean rank difference for the HM vs. WT (-4.330, p=>0.9999).

By comparing absolute turn angle between the trials for only periods when the light was on and flashed off instantaneously, a Kruskal-Wallis H test showed that there was an overall statistically significant difference in turn angle between the different genotypes across Trial 2 and Trial 3 (Trial 1: p=0.1040, Trial 2: p=0.0007, Trial 3: p=0.0061) (Figure 28). A Dunn's multiple comparisons post hoc test revealed mean rank differences between the HM vs. WT group comparison for Trial 3 (Trial 1: p=0.1500 (ns), Trial 2: p=>0.9999(ns), Trial 3: p=0.0329). There was a significant mean rank difference for the HT vs. WT comparison for Trial 2 (p=0.0038) and Trial 3 (p=0.0095). There was also a significant mean rank difference for the HM vs. HT comparison for Trial 2 (p=0.0024). Yet, there was no significant mean rank difference for the HM vs. HT comparison for trials 1 and 3 and HT vs. WT group comparison for Trial 1.

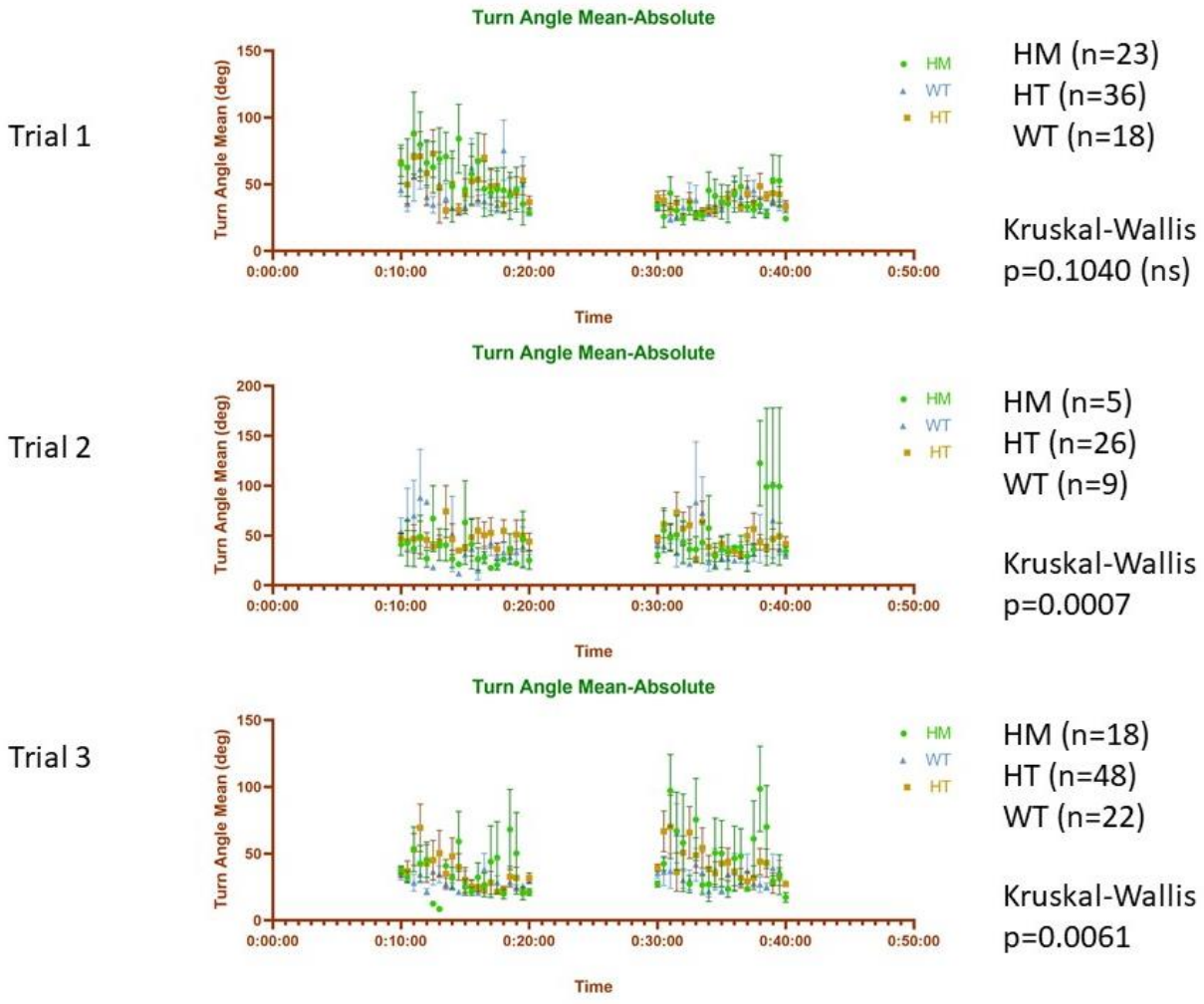

Figure 28. Absolute Turn Angle Means for *arhgef7b* Larvae Trials 1-3. Homozygotes (HM) shown in green. Heterozygotes (HT) shown in orange. Wild-type (WT) shown in blue. Turn angle means by genotype during periods when the light was turned on and flashed off instantaneously. Kruskal-Wallis H test revealed statistically significant difference in turn angle overall between the different genotypes in Trial 2 and Trial 3 (Trial 1: p=0.1040, Trial 2: p=0.0007, Trial 3: p=0.0061).

In addition, there were differences in the clockwise and counterclockwise rotation frequencies between the groups for Trial 2. A Kruskal-Wallis H test indicated that there was an overall statistically significant difference in clockwise (CW) (H=18.46 (p=<0.0001)) and counterclockwise (CCW) (H=18.99 (p=<0.0001)) turns between the different genotypes (Figures 29 and 30). Dunn's multiple comparisons post hoc tests revealed mean rank differences between various groups for both directions. There was a significant difference in the HM vs. WT group comparison (CW: 45.69, p=0.0006; CCW: 46.25, p=0.0005) and the HT vs. WT group comparison (CW:45.95, p=0.0006; CCW: 46.24, p=0.0005). Yet, there was no significant mean rank difference for the HM vs. HT group comparison for either direction (CW:-0.2574, p=>0.9999; CCW:0.01000, p=>0.9999).

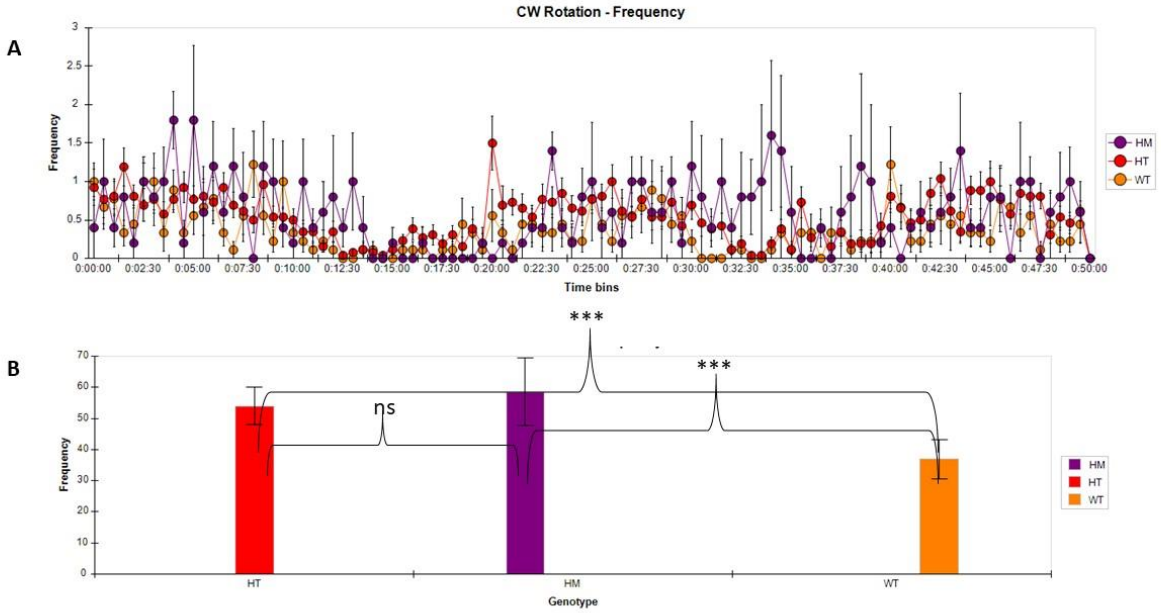

Figure 29. Clockwise (CW) rotation frequencies for *arhgef7b* Larvae Trial 2. Homozygotes (HM) shown in purple. Heterozygotes (HT) shown in red. Wild-type (WT) shown in orange. A) Clockwise rotation frequencies by genotype represented over time with each point signifying the sum of activity in a 30s time bin. B) Overall clockwise rotation frequencies by genotype. Kruskal-Wallis H test revealed statistically significant difference in rotation frequencies overall between the different genotypes, H=18.46 (p=<0.0001) (ns=p > 0.05, * = p ≤ 0.05 , **=p ≤ 0.01, ***=p ≤ 0.001, ****=p ≤ 0.0001).

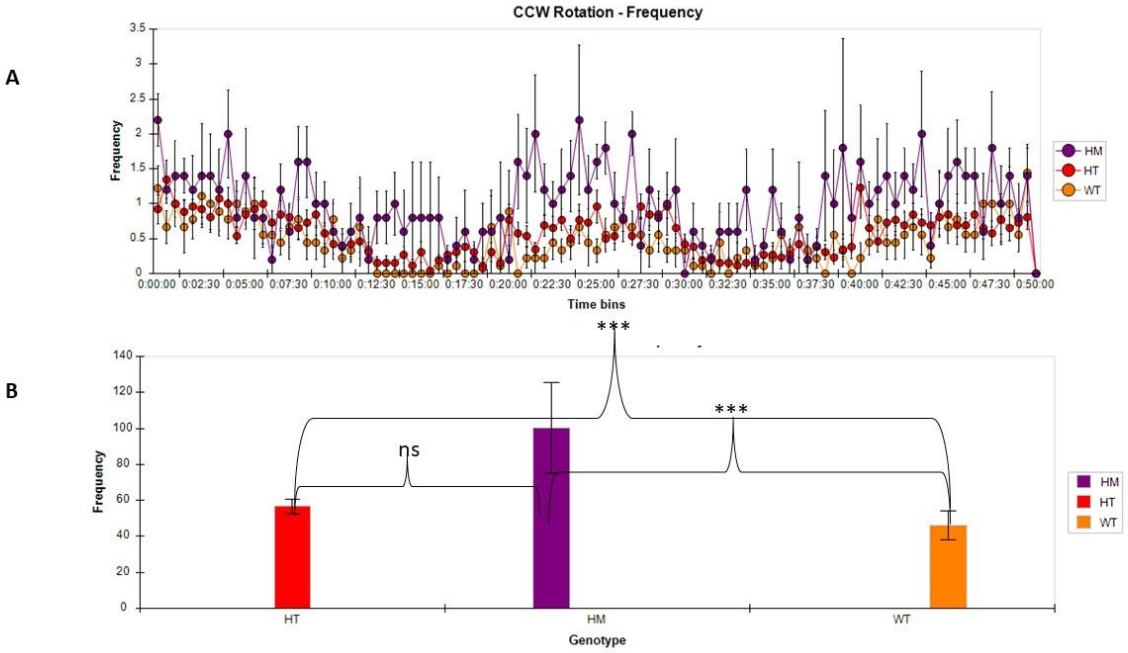

Figure 30. Counterclockwise (CCW) rotation frequencies for *arhgef7a* Larvae Trial 2. Homozygotes (HM) shown in purple. Heterozygotes (HT) shown in red. Wild-type (WT) shown in orange. A) Overall clockwise rotation frequencies by genotype. B) Counterclockwise rotation frequencies by genotype represented over time with each point signifying the sum of activity in a 30s time bin. Kruskal-Wallis H test revealed statistically significant difference in rotation frequencies overall between the different genotypes, H=18.99 (p=<0.0001) (ns=p > 0.05, * = p ≤ 0.05 , **=p ≤ 0.01, ***=p ≤ 0.001, ****=p ≤ 0.0001).

Trial 3 included 96 fish. The HRM results revealed that there were 18 homozygous (HM) fish, 48 heterzygous (HT) fish, 22 wild-type (WT) fish, and 8 fish were HRM negative or unknown. A Kruskal-Wallis H test revealed that there was an overall statistically significant difference in turn angle between the different genotypes, H=13.38 (p = 0.0012) (Figure 27). A Dunn's multiple comparisons post hoc test revealed mean rank differences between a set of groups. There was a significant difference in the HM vs. WT group comparison (-43.32, p=0.0008). However, there was no significant mean rank difference for the HM vs. HT (-22.16, p=0.1820) and HT vs. WT group comparisons (-21.16, p=0.2126).

3.3 Immunohistochemical Assays

The results of this wild-type IHC trial revealed contralateral crossing of the Mauthner hindbrain neurons (Figure 31). We had planned to conduct the same experiment on *arhgef7a* and *arhgef7b* mutants to look for aberrant ipsilateral projections, but we were unable to complete additional experiments due to COVID-19 laboratory closures.

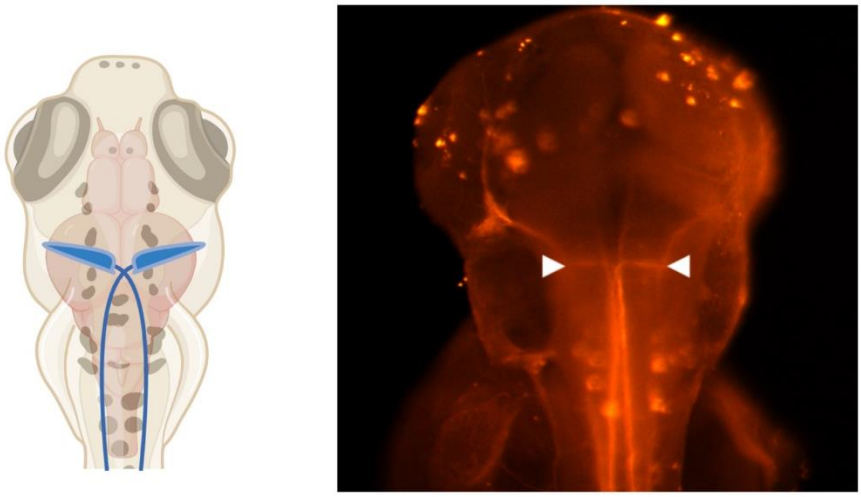

Figure 31. WT Whole-Mount IHC. Left: Schematic of Zebrafish M-cell Mauthner hindbrain neurons. M-cells shown in blue. Right: Microscope image of immunostained 72 hpf WT embryo. White arrows point to M-cells. Created with BioRender.com.

Chapter IV: General Discussion

4.1 Overview of Findings

We identified a heterozygous frameshift variant found in *ARHGEF7* (NM_001113511.1: c.1751_1752delAC, p.Asn584Thrfs*90) in the human patient family by WES that segregated with the phenotype. Since this variant maps at least 50 nucleotides upstream of the last exon junction, the variant most likely leads to mRNA decay and loss of function of this protein. Unfortunately, we were not able to conduct qRT-PCR on mutant fish to demonstrate this mode of action of *ARHGEF7* variant identified in this family. To validate the role of this variant in CMM pathogenesis, we created CRISPR-Cas9-induced mutations in the zebrafish *arhgef7a* and *arhgef7b* genes at the corresponding human mutation site. We expect that these mutants will exhibit the mirror movement-like phenotype of zebrafish *dcc* mutants reported by Jain et al. (2014) and validate the role of *ARHGEF7* in CMM.

The specific CRISPR-Cas9 genome editing-induced knockout mutations in these lines were categorized as frameshift mutations that induced premature termination codons in gene-transcribed mRNAs that could further lead to truncation of the proteins early in translation. The embryos of both the heterozygous and homozygous *arhgef7a* and *arhgef7b* lines generally developed normally compared to wild-type control embryos. However, some differences in light-induced startle responses were observed.

4.2 Mirror Movement-like Swim Defects in Zebrafish

In human CMM patients, mirror movements are most markedly produced in the hand and fingers. These movements are thought to be operated by the "cortico-motoneuronal" subsection of corticospinal neurons (Peng and Charron, 2013). In zebrafish, among other simpler vertebrates, these types of motor control functions are controlled by reticulospinal tract neurons which are analogous to the human corticospinal tract (Vulliemoz et al., 2005). The Mauthner and MiD2cm/MiD3cm/MiD3l neurons in zebrafish encompass a commissural reticulospinal hindbrain array which works to control the left and right coordination of body movements (Liu and Fetcho, 1999). Because of this, we wanted to assess the behavioral consequences of bilateral descending axonal projections hypothesized to be affected by the mutation in our *arhgef7* mutants. Since the zebrafish motor circuit functions by bilateral contractions of the trunk, it was hypothesized that mirror movement-like behaviors would be present in the form of delayed or randomized directionality of left/right lateralized body bends.

Our behavioral analyses revealed some potential for mirror movement-like swim defects in *arhgef7* zebrafish mutants. Kinematic analysis of the light startle responses of mutant *arhgef7a* and *arhgef7b* larvae showed some overall differences in relative and absolute turn angle mean. For *arhgef7a,* an overall significant mean rank difference in turn angle between all genotypes was observed across all three trials. Because the overall p-values were small across all trials, the idea that the difference in turn angle is due to random sampling can be rejected, and it can be concluded instead that the populations have different turn angle mean distributions.

The Dunn's multiple comparisons post hoc test revealed significant mean rank differences in the HM vs. WT group comparison only in Trial 1. However, the Dunn's multiple

comparisons post hoc test revealed significant mean rank differences only in the HM vs. HT group comparisons for all three trials.

For *arhgef7b*, a significant mean rank difference in relative turn angle mean between the all genotypes was observed across all three trials. Because the overall p-values were small across all trials, the idea that the difference is due to random sampling can be rejected, and it can also be concluded instead that the populations have different turn angle mean distributions.

Unlike for *arhgef7a*, the Dunn's multiple comparisons post hoc test for *arhgef7b* revealed significant mean rank differences in the HM vs. WT group comparison for Trial 1 and Trial 3 and HT vs. WT group comparison for Trial 2. The Dunn's multiple comparisons post hoc test revealed significant mean rank differences in the HM vs. HT group comparisons only for Trial 2. This difference in turn angle could be related to the increase in turning angle magnitude observed in *dcc* zebrafish mutants (Jain et al, 2014).

Additionally, there were differences in the clockwise and counterclockwise rotation frequencies between the *arhgef7b* groups for Trial 2. The Kruskal-Wallis H test indicated that there was an overall statistically significant difference in both clockwise (CW) (H=18.46 (p=<0.0001)) and counterclockwise (CCW) (H=18.99 (p=<0.0001)) turns between the different genotypes, and the Dunn's multiple comparisons post hoc test found a significant mean rank difference in the HM vs. WT group comparison (CW: 45.69, p=0.0006; CCW: 46.25, p=0.0005) and the HT vs. WT group comparison (CW:45.95, p=0.0006; CCW: 46.24, p=0.0005). The higher number of clockwise and counterclockwise rotations in our mutants could be analogous to the turns on the inappropriate body side as described by Jain et al. (2014). These results suggest that *arhgef7b* mutants may be more representative of the CMM phenotype. However, additional testing may be required to fully validate the role of *ARHGEF7* in CMM.

4.3 Conclusions

CMM is a rare genetic neurodevelopmental disorder and is on the milder spectrum of "disorders of axonal development". Though CMM represents a relatively mild phenotype, insight into its underlying molecular, genetic and pathophysiological mechanisms will have critical impact on the understanding of the more severe and disabling human disorders of axonal guidance.

The role of *ARHGEF7* has not previously been linked to the pathogenesis of CMM in humans. However, according to the Genome Aggregation Database (gnomAD), *ARHGEF7* has a probability of being loss-of-function intolerant (pLI) score of 1 (Lek et al, 2016). The database indicates that pLI scores which are closer to 1 suggest more intolerance to protein-truncating variants (Lek et al, 2016). Because the pLI of *ARHGEF7* is ≥ 0.9, *ARHGEF7* is considered extremely intolerant to loss-of-function variants (Lek et al, 2016). Since the mutation found in *ARHGEF7* (NM_001113511.1: c.1751_1752delAC, p.Asn584Thrfs*90) in our patient family is a heterozygous frameshift variant, which replaces the last 219 amino acids with 90 abnormal amino acids (Gene ID: 8874) (Figure 7), it is predicted to truncate the distal portion of the protein. However, we have not yet been able to confirm nonsense-mediated mRNA decay of our *arhgef7a* and *arhgef7b* zebrafish mutants by qRT-PCR due to the laboratory closures.

In mice, *Arhgef7* (Gene ID: 54126) homozygous knockouts are embryonic lethal. Therefore, conditional knockouts are required to assess the behavioral phenotype associated with *Arhgef7*. Because we have successfully created viable CRISPR-Cas9-induced knockout *arhgef7a* and *arhgef7b* zebrafish mutants at the identified human mutation site, these lines represent a useful model to study mirror movement-like behaviors in zebrafish.

However, there are limitations to using a zebrafish model. For example, there can be genetic redundancy in zebrafish, where two or more genes can perform the same function and knocking out of one of these genes can have no or few effect(s) on the resulting phenotype (Nowak et al., 1997). To overcome this, double knockout lines can be created to assess the resulting phenotype. We were planning to conduct detailed phenotypic analyses on double-KO *arhgef7a* and *arhgef7b* lines, however, we were not able to finish this experiment due to the halting of activities in the laboratory in relation to COVID-19.

Additionally, another limitation of this work was that we were unable to complete planned *in situ* hybridization assays on whole mount *arhgef7a* zebrafish embryos. This would have allowed us to label the complementary RNA strand and localize the mRNA in the tissue and assess the spatial and temporal expression patterns of *arhegf7a* in the zebrafish (Thisse & Thisse, 2014). A previous study has shown that *arhgef7b* is strongly expressed in the neuroepithelial cells lining the brain ventricles in zebrafish, as well as weak ubiquitous expression (Liu et al., 2007). However, the expression of *arhgef7a* has not yet been characterized.

We also planned to do overexpression assays (Objective 2) to complement the knockout assays, but we were unable to complete these studies due to COVID-19. For the overexpression assays, we wanted to inject wild-type zebrafish embryos with wild-type *ARHGEF7* and mutant *ARHGEF7* RNA and assess the resulting behavioral phenotype. If we observe a phenotype in the embryos injected with wild-type RNA but not in the embryos injected with mutant RNA, then the mutation is considered loss of function. However, if we observe a phenotype in only the embryos injected with mutant RNA but not those injected with wild-type RNA, there could be possible dominant negative effects. If there is no phenotype observed in either the embryos

injected with the wild-type or mutant RNA, we could suspect that the protein does not cause a phenotype when overexpressed or that the human protein is not recognized in the zebrafish. If we obtain this result, we will then clone and overexpress the zebrafish wild-type and mutant proteins. While we could not finish the overexpression assays due to COVID-19, these experiments were complementary. Our data from the CRISPR-Cas9-induced knockout *arhgef7a* and *arhgef7b* zebrafish mutants provides strong evidence for an important role of *ARHGEF7* in CMM pathogenesis.

Furthermore, due to variable expressivity and incomplete penetrance of CMM in humans, there could possibly be similar effects present in the zebrafish mutants. Further behavioral testing of our mutants, assessing other startle response stimuli (i.e. tactile, auditory), as well as completing the immunohistological studies looking at axonal guidance in the Mauthner hindbrain array of mutants, could enhance our understanding of the function of the heterozygous frameshift variant found in *ARHGEF7* in the human patient family. Evaluating our double *arhgef7a/arhgef7b* zebrafish knockouts could also prove useful in further characterizing the mirror movement-like phenotype.

Additionally, discovery of novel CMM genes is very important to patients, as it allows for a more accurate diagnosis and genetic counseling. Furthermore, understanding the disease mechanisms of CMM and the underlying deficits of lateralization is critical for developing novel strategies to promote guidance and re-wiring of damaged axons, and targeted rehabilitation approaches that can also be used in common neurologic connectivity disorders, such as stroke and cerebral palsy. Moreover, this project has worked to uncover and better understand the role of *ARHGEF7* as a gene potentially contributing to the pathogenesis of CMM.

References

Ahmed I, Mittal K, Sheikh TI, Vasli N, Rafig MA, Mikhailov A, et al. Identification of a homozygous splice site mutation in the dynein axonemal light chain 4 gene on 22q13.1 in a large consanguineous family from Pakistan with congenital mirror movement disorder. *Hum Genet* Aug 7 2014;133(11):1419–29.

Anderson JL, Mulligan TS, Shen M-C, Wang H, Scahill CM, Tan FJ, et al. (2017) mRNA processing in mutant zebrafish lines generated by chemical and CRISPR-mediated mutagenesis produces unexpected transcripts that escape nonsense-mediated decay. PLoS Genet 13(11): e1007105. https://doi.org/10.1371/journal.pgen.1007105

Bonnet C, Roubertie A, Doummar D, Bahi-Buisson N, Cochen de Cock V, Roze E. Developmental and benign movement disorders in childhood. *Mov Disord*. 2010;25:1317–34.

Brancati F, Dallapiccola B, Valente EM. Joubert syndrome and related disorders. *Orphanet journal of rare diseases*. 2010;5(1):20-20. doi:10.1186/1750-1172-5-20

Brandao P, et al. Congenital mirror movements: lack of decussation of pyramids. *Brain*. 2014;137:e292. doi: 10.1093/brain/awu073.

Brustein E, Saint-Amant L, Buss RR, Chong M, Mcdearmid JR, Drapeau P. Steps during the development of the zebrafish locomotor network. *Journal of Physiology-Paris*. 2003;97(1):77-86. doi:10.1016/j.jphysparis.2003.10.009

Bustelo, XR, Sauzeau, V, & Berenjeno, IM. (2007). GTP-binding proteins of the Rho/Rac family: regulation, effectors and functions in vivo. *BioEssays : news and reviews in molecular, cellular and developmental biology, 29*(4), 356–370. doi:10.1002/bies.20558

Burgess HA, Granato M (2007b) Modulation of locomotor activity in larval zebrafish during

light adaptation. *J Exp Biol* 210:2526–2539, doi:10.1242/jeb.003939, pmid:17601957.

Chen Z, Lee H, Henle SJ, Cheever TR, Ekker SC, Henley JR. Primary neuron culture for nerve growth and axon guidance studies in zebrafish (Danio rerio). *PLoS One*. 2013;8(3):e57539. doi:10.1371/journal.pone.0057539

Cincotta M, Ziemann U. Neurophysiology of unimanual motor control and mirror movements [Review] *Clin Neurophysiol*. 2008;119:744–62.

Colwill, RM, Creton, R. "Locomotor Behaviors in Zebrafish (Danio Rerio) Larvae." *Behavioural Processes* 86, no. 2 (2011): 222–29. https://doi.org/10.1016/j.beproc.2010.12.003.

Colwill RM, Creton R. Imaging escape and avoidance behavior in zebrafish larvae. *Rev Neurosci*. 2011;22(1):63–73. doi:10.1515/RNS.2011.008

Congenital mirror movement disorder. *Genetics Home Reference (GHR).* April, 2015; http://ghr.nlm.nih.gov/condition/congenital-mirror-movement-disorder.

Cox BC, Cincotta M, Espay AJ. Mirror movements in movement disorders: a review. *Tremor Other Hyperkinet Mov (N Y)*. 2012;2:tre-02-59-398-1. doi:10.7916/D8VQ31DZ

Demirayak P, Onat OE, Gevrekci AÖ, Gülsüner S, Uysal H, Bilgen RS, Doerschner K, et al. Abnormal subcortical activity in congenital mirror movement disorder with RAD51 mutation. *Diagn Interv Radiol*. November, 2018; 24(6):392-401. https://www.ncbi.nlm.nih.gov/pmc/articles/PMC6223827/.

Depienne C, et al. A novel DCC mutation and genetic heterogeneity in congenital mirror movements. *Neurology.* 2011;76(3):260–264. doi: 10.1212/WNL.0b013e318207b1e0.

Depienne C, et al. RAD51 haploinsufficiency causes congenital mirror movements in humans. *Am J Hum Genet*. 2012;90(2):301–307. doi: 10.1016/j.ajhg.2011.12.002.

Farmer S, Ingram D, Stephens J (1990) Mirror movements studied in a patient with Klippel-Feil syndrome. The Journal of physiology 428:467-484

Fasano A, Bologna M, Iezzi E, et al. Congenital Mirror Movements in a New Italian Family. *Mov Disord Clin Pract*. 2014;1(3):180–187. Published 2014 Jul 28. doi:10.1002/mdc3.12066

Ferland RJ, Eyaid W, Collura RV, Tully LD, Hill RS, Al-Nouri D, Al-Rumayyan A, Topcu M, Gascon G, Bodell A, Shugart YY, Ruvolo M, Walsh CA (2004): Abnormal cerebellar development and axonal decussation due to mutations in AHI1 in Joubert syndrome. *Nat Genet* 36:1008–1013.

Finger JH, Bronson RT, Harris B, Johnson K, Przyborski SA, Ackerman SL (2002) The netrin 1 receptors Unc5h3 and Dcc are necessary at multiple choice points for the guidance of corticospinal tract axons. *Journal of Neuroscience* 22:10346-10356.

Galléa C, Popa T, Billot S, Méneret A, Depienne C, Roze E. Congenital mirror movements: a clue to understanding bimanual motor control. *Journal of Neurology*. 2011;258(11):1911-1919. doi:10.1007/s00415-011-6107-9

Gore AV, Monzo K, Cha YR, Pan W, Weinstein BM. Vascular development in the zebrafish. *Cold Spring Harb Perspect Med*. 2012;2(5):a006684. doi:10.1101/cshperspect.a006684

Gunderson H, Solitare GB (1968) Mirror movements in patients with the Klippel-Feil syndrome: neuropathologic observations. Archives of neurology 18:675-679

Hardelin J-P and Young J. Kallmann syndrome. Orphanet. June, 2013; http://www.orpha.net/consor/cgi-bin/OC_Exp.php?lng=en&Expert=478.

Howe, K, Clark, MD, Torroja, F, Torrance, J, Berthelot, C, Muffato, M, Collins, JE,

Humphray, S, McLaren, K, Matthews, L, McLaren, S, Sealy, I, Caccamo, M, Churcher, C, Scott, C, Barrett, JC, Koch, R, Rauch, GJ, White, S, Chow, W, … Stemple, DL (2013). The zebrafish reference genome sequence and its relationship to the human genome. *Nature*, *496*(7446), 498–503. https://doi.org/10.1038/nature12111

Jain RA, Bell H, Lim A, Chien CB, Granato M. Mirror movement-like defects in startle behavior of zebrafish dcc mutants are caused by aberrant midline guidance of identified descending hindbrain neurons. *The Journal of Neuroscience: The Official Journal Of The Society For Neuroscience*. 2014;34(8):2898-2909. doi:10.1523/JNEUROSCI.2420-13.2014

Jamuar SS, Schmitz-Abe K, D'Gama AM, et al. Biallelic mutations in human dcc cause developmental split-brain syndrome. *Nature genetics*. 2017;49(4):606-612. doi:10.1038/ng.3804

Jen JC, Chan WM, Bosley TM, et al., " Mutations in a human ROBO gene disrupt hindbrain axon pathway crossing and morphogenesis, " *Science*. Jun 4 2004;304(5676):1509–1513.

Kalueff, AV, Gebhardt, M, Stewart, AM, Cachat, JM, Brimmer, M, Chawla, JS, … Zebrafish Neuroscience Research Consortium (2013). Towards a comprehensive catalog of zebrafish behavior 1.0 and beyond. *Zebrafish*, *10*(1), 70–86. doi:10.1089/zeb.2012.0861

Kandel, ER, Schwartz, JH, Jessell, TM. (2000). Principles of neural science (4th ed.). New York: McGraw-Hill, Health Professions Division.

Kanungo J, Lantz S, Paule MG. In vivo imaging and quantitative analysis of changes in axon length using transgenic zebrafish embryos. *Neurotoxicol Teratol*. 2011;33(6):618–623. doi:10.1016/j.ntt.2011.08.013

Karaca E, Yuregir OO, Bozdogan ST, et al. Rare variants in the notch signaling pathway describe a novel type of autosomal recessive Klippel-Feil syndrome. *Am J Med Genet A*. 2015;167A(11):2795-2799. doi:10.1002/ajmg.a.37263

Keino-Masu K, et al. Deleted in Colorectal Cancer (DCC) encodes a netrin receptor. *Cell*. 1996;87(2):175–185. doi: 10.1016/S0092-8674(00)81336-7.

Kennedy TE, Serafini T, de la Torre JR, Tessier-Lavigne M. Netrins are diffusible chemotropic factors for commissural axons in the embryonic spinal cord. *Cell*. 1994;78(3):425–435. doi: 10.1016/0092-8674(94)90421-9.

Korenbaum, E, Rivero, F. (Sep 2002). "Calponin homology domains at a glance". *J Cell Sci*. 115 (Pt 18): 3543â€“5. CiteSeerX 10.1.1.608.8653. doi:10.1242/jcs.00003. PMID 12186940.

Kurochkina, N, & Guha, U. (2013). SH3 domains: modules of protein-protein interactions. *Biophysical reviews*, *5*(1), 29–39. doi:10.1007/s12551-012-0081-z

Krams M, Quinton R, Ashburner J, Friston K, Frackowiak R, Bouloux P-M, Passingham R (1999) Kallmann's syndrome mirror movements associated with bilateral corticospinal tract hypertrophy. Neurology 52:816-816.

Krams M, Quinton R, Mayston M, Harrison L, Dolan R, Bouloux P, Stephens J, Frackowiak R, Passingham R (1997) Mirror movements in X-linked Kallmann's syndrome. II. A PET study. Brain: a journal of neurology 120:1217-1228.

Lan CC, Tang R, Un San Leong I, Love DR. Quantitative real-time rt-pcr (qrt-pcr) of zebrafish transcripts: optimization of rna extraction, quality control considerations, and data analysis. *Cold spring harbor protocols*. 2009;2009(10):5314. doi:10.1101/pdb.prot5314

Lei, X, Deng, L, Liu, D, Liao, S, Dai, H, Li, J, … Li, T. (2018). *ARHGEF7* promotes

metastasis of colorectal adenocarcinoma by regulating the motility of cancer cells. *International Journal of Oncology*. doi: 10.3892/ijo.2018.4535

Leinsinger, GL, Heiss, DT, Jassoy, AG, Pfluger, T, Hahn, K, Danek, A. Persistent mirror movements: functional MR imaging of the hand motor cortex *Radiology*, 203 (1997), pp. 545-552.

Lek, M., Karczewski, K., Minikel, E. *et al.* Analysis of protein-coding genetic variation in 60,706 humans. *Nature* 536**,** 285–291 (2016). https://doi.org/10.1038/nature19057

Li MZ, Elledge SJ. SLIC: A Method for Sequence- and Ligation-Independent Cloning. *Methods in Molecular Biology Gene Synthesis*. 2012:51-59. doi:10.1007/978-1-61779-564-0_5

Li JY, Lai PH, Chen R. Transcallosal inhibition in patients with callosal infarction. *Journal of neurophysiology*. 2013;109(3):659-665. doi:10.1152/jn.01044.2011

Liu J, D Fraser S, Faloon P, et al. A βPix–Pak2a signaling pathway regulates cerebral vascular stability in zebrafish. Vol 104. ; 2007:13990-5. 10.1073/pnas.0700825104.

Liu, J, Zeng, L, Kennedy, RM, Gruenig, NM, and Childs, SJ. (2012) betaPix plays a dual role in cerebral vascular stability and angiogenesis and interacts with integrin alphavbeta8. *Developmental Biology*. 363(1):95-105.

López Tobón, A., Suresh, M., Jin, J., Vitriolo, A., Pietralla, T., Tedford, K., Püschel, A. W. (2018). The guanine nucleotide exchange factor Arhgef7/βPix promotes axon formation upstream of TC10. *Scientific Reports*, 8, 8811. http://doi.org/10.1038/s41598-018-27081-1

Maegaki Y, Seki A, Suzaki I, et al. Congenital mirror movement: a study of functional mri and transcranial magnetic stimulation. *Developmental Medicine & Child Neurology*. 2007;44(12):838-843. doi:10.1111/j.1469-8749.2002.tb00774.x

Marsden KC, Granato M. In Vivo Ca2 Imaging Reveals that Decreased Dendritic Excitability Drives Startle Habituation. *Cell Reports*. 2015;13(9):1733-1740. doi:10.1016/j.celrep.2015.10.060

Marsh AP, Heron D, Edwards TJ, et al. Mutations in DCC cause isolated agenesis of the corpus callosum with incomplete penetrance. *Nat Genet*. 2017;49(4):511-514. doi:10.1038/ng.3794

Marsh APL, Edwards TJ, Galea C, et al. DCC mutation update: Congenital mirror movements, isolated agenesis of the corpus callosum, and developmental split brain syndrome. *Hum Mutat*. 2018;39(1):23-39. doi:10.1002/humu.23361

Mayston MJ, Harrison LM, Stephens JA (1999) A neurophysiological study of mirror movements in adults and children. Annals of neurology 45:583-594.

Mayston MJ, Harrison LM, Quinton R, Stephens J, Krams M, Bouloux P (1997) Mirror movements in X-linked Kallmann's syndrome. I. A neurophysiological study. Brain: a journal of neurology 120:1199-1216.

McDonald, J.H. 2014. *Handbook of Biological Statistics* (3rd ed.). *Sparky House Publishing*, Baltimore, Maryland.

Méneret A, Depienne C, Riant F, et al. Congenital mirror movements: mutational analysis of RAD51 and DCC in 26 cases. *Neurology*. 2014;82(22):1999–2002. doi:10.1212/WNL.0000000000000477

Méneret A, Trouillard O, Depienne C, Roze E. Congenital Mirror Movements. *GeneReviews*. March, 2015; http://www.ncbi.nlm.nih.gov/books/NBK279760/.

Méneret A, Franz EA, Trouillard O, et al. Mutations in the netrin-1 gene cause congenital mirror

movements. *Journal of Clinical Investigation*. 2017;127(11):3923-3936. doi:10.1172/JCI95442

Moriya H. Quantitative nature of overexpression experiments. *Mol Biol Cell*. 2015;26(22):3932–3939. doi:10.1091/mbc.E15-07-0512

Nowak, M., Boerlijst, M., Cooke, J. *et al.* Evolution of genetic redundancy. *Nature* 388, 167–171 (1997). https://doi.org/10.1038/40618

Nugent AA, Kolpak AL, Engle EC. Human disorders of axon guidance. *Current opinion in neurobiology*. 2012;22(5):837-843. doi:10.1016/j.conb.2012.02.006

O'Malley DM, Kao YH, Fetcho JR. Imaging the functional organization of zebrafish hindbrain segments during escape behaviors. *Neuron*. 1996;17:1145–1155. doi: 10.1016/S0896-6273(00)80246-9.

Observation Chamber - Zebrafish research: DanioVision. Observation Chamber - Zebrafish research | DanioVision. https://www.noldus.com/daniovision. Accessed January 13, 2020.

Peng J, Charron F. Lateralization of motor control in the human nervous system: genetics of mirror movements. *Curr Opin Neurobiol*. 2012;23:109–118. doi: 10.1016/j.conb.2012.08.007.

Prelich G. Gene overexpression: uses, mechanisms, and interpretation. *Genetics*. 2012;190(3):841–854. doi:10.1534/genetics.111.136911

Samarut É, Lissouba A, Drapeau P. A simplified method for identifying early CRISPR-induced indels in zebrafish embryos using High Resolution Melting analysis. *BMC Genomics*. 2016;17:547. Published 2016 Aug 4. doi:10.1186/s12864-016-2881-1

Santos D, Monteiro SM, Luzio A. General Whole-Mount Immunohistochemistry of Zebrafish

(Danio rerio) Embryos and Larvae Protocol. *Methods in Molecular Biology Teratogenicity Testing*. 2018:365-371. doi:10.1007/978-1-4939-7883-0_19

Shibasaki H, Sadato N, Lyshkow H, Yonekura Y, Honda M, Nagamine T, Suwazono S, Magata Y, Ikeda A, Miyazaki M, Fukuyama H, Asato R, Konishi J (1993) Both primary motor cortex and supplementary motor area play an important role in complex finger movement. Brain 116:1387-1398.

Shimazaki T, Tanimoto M, Oda Y, Higashijima SI. Behavioral role of the reciprocal inhibition between a pair of mauthner cells during fast escapes in zebrafish. *The journal of neuroscience : the official journal of the society for neuroscience*. 2019;39(7):1182-1194. doi:10.1523/JNEUROSCI.1964-18.2018

"Site-Directed Mutagenesis." *Hawleys Condensed Chemical Dictionary*, 2007. https://doi.org/10.1002/9780470114735.hawley14580.

Srour M., Riviere J. B., Pham J. M., Dube M. P., Girard S., Morin S., Dion P. A., Asselin G., Rochefort D., Hince P., et al. (2010). Mutations in DCC cause congenital mirror movements. *Science* 328, 592.

Srour M, Schwartzentruber J, Hamdan FF, Ospina LH, Patry L, Labuda D, Massicotte C, Dobrzeniecka S, Capo-Chichi JM, Papillon-Cavanagh S, Samuels ME, Boycott KM, Shevell MI, Laframboise R, Désilets V; FORGE Canada Consortium, Maranda B, Rouleau GA, Majewski J, Michaud JL. Mutations in C5ORF42 cause Joubert syndrome in the French Canadian population. *Am J Hum Genet*. 2012;90(4):693-700.

Srour M, Hamdan FF, Schwartzentruber JA, Patry L, Ospina LH, Shevell MI, Désilets V, Dobrzeniecka S, Mathonnet G, Lemyre E, Massicotte C, Labuda D, Amrom D, Andermann E, Sébire G, Maranda B, Consortium FC, Rouleau GA, Majewski J, Michaud

JL. Mutations in TMEM231 cause Joubert syndrome in French Canadians. *J Med Genet*. 2012 Oct;49(10):636-41.

Turner RS, Grafton ST, Votaw JR, Delong MR, Hoffman JM (1998) Motor subcircuits mediating the control of movement velocity: a PET study. *Journal of Neurophysiology* 80:2162-2176.

Thisse, B., & Thisse, C. (2014). In Situ Hybridization on Whole-Mount Zebrafish Embryos and Young Larvae. *Methods in Molecular Biology In Situ Hybridization Protocols*, 53–67. doi: 10.1007/978-1-4939-1459-3_5

Vector Database. Addgene. https://www.addgene.org/vector-database/2295/. Accessed January 13, 2020.

Vulliemoz S, Raineteau O, Jabaudon D. Reaching beyond the midline: why are human brains cross wired? *The Lancet Neurology*. 2005;4(2):87-99. doi:10.1016/s1474-4422(05)00990-7

Welniarz Q, Dusart I, Gallea CC, Roze E. One hand clapping: lateralization of motor control. *Frontiers in Neuroanatomy* 2015;9. doi:10.3389/fnana.2015.00075.

Woods BT, Teuber HL. (1978) Mirror movements after childhood hemiplegia. *Neurology* 28: 1152–8.

Zhou W, Li X, Premont RT. Expanding functions of GIT Arf GTPase-activating proteins, PIX Rho guanine nucleotide exchange factors and GIT–PIX complexes. *Journal of Cell Science*. 2016;129(10):1963-1974. doi:10.1242/jcs.179465

Zhu, K, Debreceni, B, Bi, F, & Zheng, Y. (2001). Oligomerization of DH domain is essential for Dbl-induced transformation. *Molecular and cellular biology*, *21*(2), 425–437. doi:10.1128/MCB.21.2.425-437.2001